# NAVAL POSTGRADUATE SCHOOL

## MONTEREY, CALIFORNIA

# THESIS

**MOLYBDENUM CARBIDE SYNTHESIS USING PLASMAS FOR FUEL CELLS**

by

John J. Lugge

June 2013

| | |
|---|---|
| Thesis Advisor: | Jonathan Phillips |
| Thesis Co-Advisor: | Claudia Luhrs |

**Approved for public release; distribution is unlimited**

THIS PAGE INTENTIONALLY LEFT BLANK

| REPORT DOCUMENTATION PAGE | | *Form Approved OMB No. 0704–0188* |
|---|---|---|
| Public reporting burden for this collection of information is estimated to average 1 hour per response, including the time for reviewing instruction, searching existing data sources, gathering and maintaining the data needed, and completing and reviewing the collection of information. Send comments regarding this burden estimate or any other aspect of this collection of information, including suggestions for reducing this burden, to Washington headquarters Services, Directorate for Information Operations and Reports, 1215 Jefferson Davis Highway, Suite 1204, Arlington, VA 22202–4302, and to the Office of Management and Budget, Paperwork Reduction Project (0704–0188) Washington DC 20503. | | |
| **1. AGENCY USE ONLY** *(Leave blank)* | **2. REPORT DATE** June 2013 | **3. REPORT TYPE AND DATES COVERED** Master's Thesis |
| **4. TITLE AND SUBTITLE** MOLYBDENUM CARBIDE SYNTHESIS USING PLASMAS FOR FUEL CELLS | | **5. FUNDING NUMBERS** |
| **6. AUTHOR(S)** John J. Lugge | | |
| **7. PERFORMING ORGANIZATION NAME(S) AND ADDRESS(ES)** Naval Postgraduate School Monterey, CA 93943–5000 | | **8. PERFORMING ORGANIZATION REPORT NUMBER** |
| **9. SPONSORING /MONITORING AGENCY NAME(S) AND ADDRESS(ES)** N/A | | **10. SPONSORING/MONITORING AGENCY REPORT NUMBER** |
| **11. SUPPLEMENTARY NOTES** The views expressed in this thesis are those of the author and do not reflect the official policy or position of the Department of Defense or the U.S. Government. IRB Protocol number ____N/A____. | | |
| **12a. DISTRIBUTION / AVAILABILITY STATEMENT** Approved for public release; distribution is unlimited | | **12b. DISTRIBUTION CODE** |

**13. ABSTRACT (maximum 200 words)**

Currently, carbon is the preferred support material for platinum catalyst particles used in polymer electrolyte fuel cells (PEFCs). Carbon possesses qualities needed for a fuel cell catalyst: high surface area and conductivity, but is unacceptable as it is prone to oxidization by carbon dioxide in the fuel cell environment. Molybdenum Carbides is known to have the required conductivity. However, making $Mo_2C$ with sufficient surface area and with stabilized platinum remains a materials challenge. In this work a novel approach, a variation on the Aerosol-Through-Plasma (ATP) method was employed for making $Mo_2C$ with high surface area and stable supported platinum particles. An ammonium molybdate precursor was processed through different ATP conditions to generate the catalyst. These particles were then characterized using X-ray diffraction and SEM techniques in order to produce a support material with the highest concentration of $Mo_2C$. Using the ideal conditions for the ATP, precursor was loaded with platinum and then processed through the ATP. This sample was then characterized using X-ray and SEM techniques to insure that the material was suitable prior to testing the electrochemical properties under PEFC operating conditions. The results were then compared to other leading support catalysis.

| **14. SUBJECT TERMS** Molybdenum Carbines, Fuel Cells, Aerosol-Through-Plasma, Catalysts | | | **15. NUMBER OF PAGES** 89 |
|---|---|---|---|
| | | | **16. PRICE CODE** |
| **17. SECURITY CLASSIFICATION OF REPORT** Unclassified | **18. SECURITY CLASSIFICATION OF THIS PAGE** Unclassified | **19. SECURITY CLASSIFICATION OF ABSTRACT** Unclassified | **20. LIMITATION OF ABSTRACT** UU |

NSN 7540–01–280–5500

Standard Form 298 (Rev. 2–89)
Prescribed by ANSI Std. 239–18

THIS PAGE INTENTIONALLY LEFT BLANK

**MOLYBDENUM CARBIDE SYNTHESIS USING PLASMAS FOR FUEL CELLS**

John J. Lugge
Lieutenant, United States Navy
B.S. Mechanical Engineering, California Maritime Academy, 2009

Submitted in partial fulfillment of the
requirements for the degree of

**MASTER OF SCIENCE IN MECHANICAL ENGINEERING**

from the

**NAVAL POSTGRADUATE SCHOOL**
**June 2013**

Author:          John J. Lugge

Approved by:     Jonathan Phillips
                 Thesis Advisor

                 Claudia Luhrs
                 Thesis Co-Advisor

                 Knox Millsaps
                 Chair, Department of Mechanical and Aerospace Engineering

iii

THIS PAGE INTENTIONALLY LEFT BLANK

# ABSTRACT

Currently, carbon is the preferred support material for platinum catalyst particles used in polymer electrolyte fuel cells (PEFCs). Carbon possesses qualities needed for a fuel cell catalyst: high surface area and conductivity, but is unacceptable as it is prone to oxidization by carbon dioxide in the fuel cell environment. Molybdenum Carbides is known to have the required conductivity. However, making Mo2C with sufficient surface area and with stabilized platinum remains a materials challenge. In this work a novel approach, a variation on the Aerosol-Through-Plasma (ATP) method was employed for making Mo2C with high surface area and stable supported platinum particles. An ammonium molybdate precursor was processed through different ATP conditions to generate the catalyst. These particles were then characterized using X-ray diffraction and SEM techniques in order to produce a support material with the highest concentration of Mo2C. Using the ideal conditions for the ATP, precursor was loaded with platinum and then processed through the ATP. This sample was then characterized using X-ray and SEM techniques to insure that the material was suitable prior to testing the electrochemical properties under PEFC operating conditions. The results were then compared to other leading support catalysis.

THIS PAGE INTENTIONALLY LEFT BLANK

# TABLE OF CONTENTS

THIS PAGE INTENTIONALLY LEFT BLANK

# LIST OF FIGURES

# LIST OF TABLES

THIS PAGE INTENTIONALLY LEFT BLANK

# LIST OF ACRONYMS AND ABBREVIATIONS

| | |
|---|---|
| ATP | Aerosol-Through-Plasma |
| $A/cm^2$ | Amps per Centimeter Squared |
| Å | Angstrom |
| ads | Adsorbtion |
| $(NH_4)_6Mo_7O_{24}\ 4H_2O$ | Ammonium Molybdate Tetrahydrate |
| $(NH_4)_2MoO_4$ | Ammonium Molybdate |
| $^oC$ | Celsius |
| CO | Carbon Monoxide |
| $CO_2$ | Carbon Dioxide |
| DOE | Department of Energy |
| $/m2 | Dollars per Meters Squared |
| $/kW | Dollars per Kilowatt |
| EDS | Energy-Dispersive Spectrometer |
| GHz | Gega Hertz |
| $g/m^2$ | Grams per Meters Squared |
| g/min | Grams per Minute |
| H | Hydrogen |
| $H_2$ | Hydrogen Gas |
| $H_2S$ | Hydrogen Sulfide |
| K | Kelvin |
| kV | Kilovolt |
| KeV | Kilo Electron Volt |
| LANL | Los Alamos National Lab |
| MeV | Mega Electron Volt |
| μm | Micrometer |
| mA | Milliamps |
| mV | Millivolt |
| MoC or $Mo_2C$ | Molybdenum Carbide |
| $N_2$ | Nitrogen Gas |
| nm | Nanometer |

| | |
|---|---|
| $\Omega/cm^2$ | Ohms per Centimeter Squared |
| O | Oxygen |
| PEM | Proton Exchange Membrane |
| PFSA | Perfluorosulfonic Acid |
| Pt | Platinum |
| RF | Radio Frequency |
| S/cm | Siemens per Centimeter |
| $C_2F_4–C_7F_{13}O_2–(SO_3H)$ | Sulfonated Tetrafouroethylene Fluoropolymer-Copolymer |
| SEM | Scanning Electron Microscope |
| x | Times |
| XRD | X-Ray Diffraction |
| ′ | Foot or Feet |
| ″ | Inch or Inches |

# ACKNOWLEDGMENTS

THIS PAGE INTENTIONALLY LEFT BLANK

# I. INTRODUCTION

## A. DRIVING FORCE FOR FUEL CELL DEVELOPMENT

Today the predominant means to produce electrical and mechanical energy to propel or energize equipment comes from the use of combustion engines that use fossil fuels. Over the last several decades the cost of fossil fuel and the demand has increased. This has led to an increase in dependence on fossil fuels to the point that it has been seen as a critical resource for national security [1]. In addition, there is overwhelming, although not unanimous, agreement within the scientific community that the byproducts from combustion are causing climate change. This has seen so much attention that President Obama identified the need to reduce the dependence on fossil fuels in an effort to curb climate change in his 2013 State of the Union Address [2].

With congress passing the Energy Policy Act of 2005, the Energy Independence and Security Act of 2007, and the American Recover and Reinvestment Act, there has been substantial pressure put on the Department of Energy (DOE) to respond to these challenges. DOE has determined that fuel cells are potentially an efficient and clean alternative to fossil fuels. Indeed, if hydrogen is created electrically from renewable sources (nuclear, solar, wind, etc.) $CO_2$ emissions from vehicles will be reduced by almost 100%. Even if hydrogen is generated from reformed hydrocarbons (e.g., methanol) best estimates are that $CO_2$ emissions will be reduced by more than 80%. DOE has identified and outlined key factors, including technological issues, required for making fuel cells a viable solution [3].

There are three technological barriers that prevent fuel cells from being competitive with current technologies. The first is the issue of fuel storage and capacity. A compact, light-weight storage system is required to store the required reactants so vehicles can exceed a 300-mile driving range without minimizing performance. The second is to improve the durability and service life of fuel cells. For vehicular applications fuel cells will need to be able to provide a minimum of 5,000 operating hours and for stationary applications a minimum of 60,000 operating hours. The third,

and probably the most important barrier, is cost. The cost of constructing, operating, creating hydrogen for fuel, and storing the fuel needs to be lowered [3].

## B.     REVIEW ON FUEL CELL TECHNOLOGY

Fuel Cells can be seen as an energy conversion device that directly converts chemical energy into electrical energy. It accomplishes this conversion in a similar manner to a battery. In a battery there are two electrodes. One electrode is called an anode and the other is a cathode. These electrodes do not physically contact one another, but are often immersed in an electrolyte that allows for electrical charges to flow freely. When the electrodes are connected to an external source several processes occur. At the anode an oxidation reaction occurs. Ions from the electrolyte combine with the anode producing a new substance and releasing electrons. Similarly, at the cathode a reducing reaction occurs absorbing the electrons that were given off by the anode [4].

For fuel cells it is the anodic oxidation of hydrogen at the anode and the reduction of oxygen at the cathode that produce this flow. Unlike batteries, the fuel for the Fuel Cell, the reactants (the fuel and oxidants) can be stored outside of where the electrodes and reactions occur. It is feasible that efficiencies approaching 70% are possible depending on the configuration and set up used. Figure 1 compares the specific power and specific energy for a variety of energy conversion and storage systems [5]. Furthermore these reactions can be powered not by fossil fuel but by fuel (hydrogen) generated with renewable technologies, thus reducing emissions and U.S. dependence on imported oil [3].

Currently there are five generic categories of practical fuel cell set ups. These are Phosphoric Acid Fuel Cells, Proton Exchange Membrane Fuel Cells, Molten Carbonate Fuel Cells, Solid Oxide Fuel Cell, and Direct and Indirect Methanol Fuel Cell [5]. For this study only the Proton Exchange Membrane Fuel Cell is relevant due to its construction and operation characteristics.
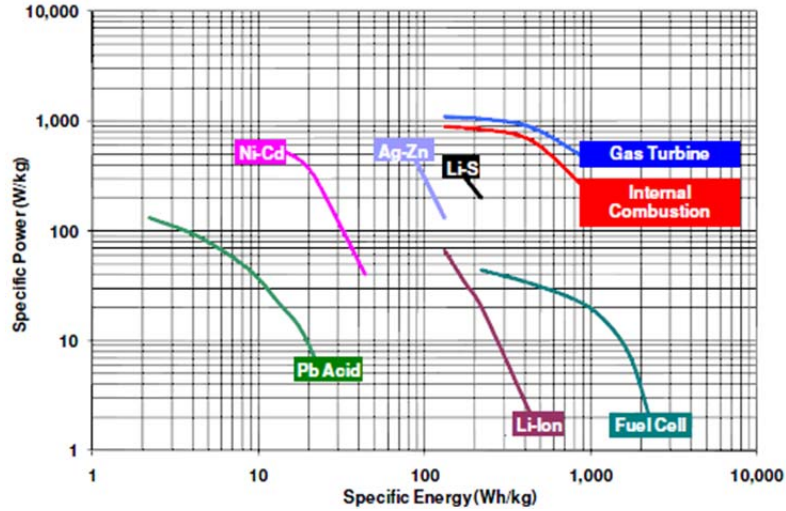
Figure 1.   Specific power vs. specific energy for energy conversion and storage system. From [5]

Willard Thomas Grubb and Leonard Niedrach of General Electric invented the proton Exchange Membrane (PEM) fuel cell in the 1960s. PEM fuel cells were used in the Gemini space craft, and recently used on the Type 212a German submarine [5]. There are several reasons why this fuel cell has received greater interest over the years. Its high power density, short start-up time, and ability to rapidly respond to varying loads make it an ideal candidate for use in vehicles [6]. In addition, PEM fuel cells operate at lower temperatures, typically 50 to 100$^o$C, compared to other fuel cells making it safer [5], [6].

Typical fuel and oxidizer for this system are hydrogen and oxygen. These reactants can be stored in a variety of ways such as a gas, liquid, or in the case of hydrogen as a hydride (example: ion-titanium-hydride). Below are three equations showing the anodic oxidation of the hydrogen at the anode, the reduction of oxygen at the cathode, and the overall reaction of the system [5].

$$H_2(g) \rightarrow 2H^+ + 2e$$
$$E_o = 0V(SHE) \tag{1}$$

$$O_2(g) + 2H^+ + 2e \rightarrow H_2O(l)$$
$$E_0 = +1.23V(SHE) \tag{2}$$

$$2H_2(g) + O_2(g) \rightarrow 2H_2O(l)$$
$$\Delta E = +1.23V \tag{3}$$

3
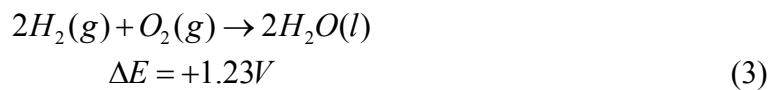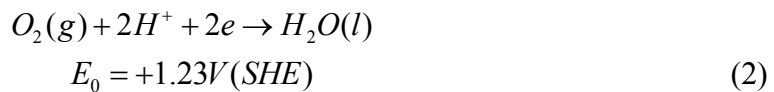
PEM fuel cells in the simplest form consist of two flow field plates, membrane-electrode assembly (MEA), and seals that are all sandwiched together. These parts form one cell and the cells can be stacked together in series with other cells to form a stack of cells [6]. Figure 2 shows a typical PEM fuel cell, and Figure 3 illustrates the sandwiched internal components [5], [6].
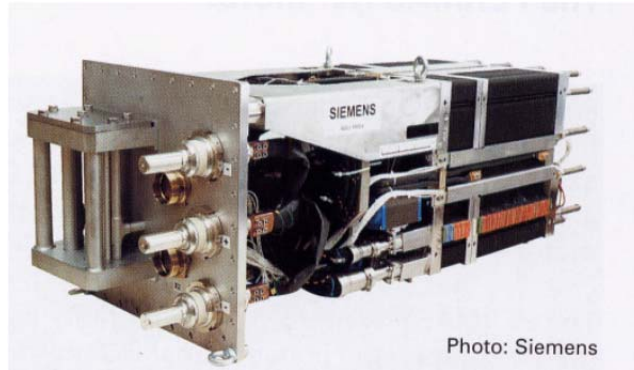


Figure 2.    PEM fuel cell used on the Type 212a submarine. From [5].
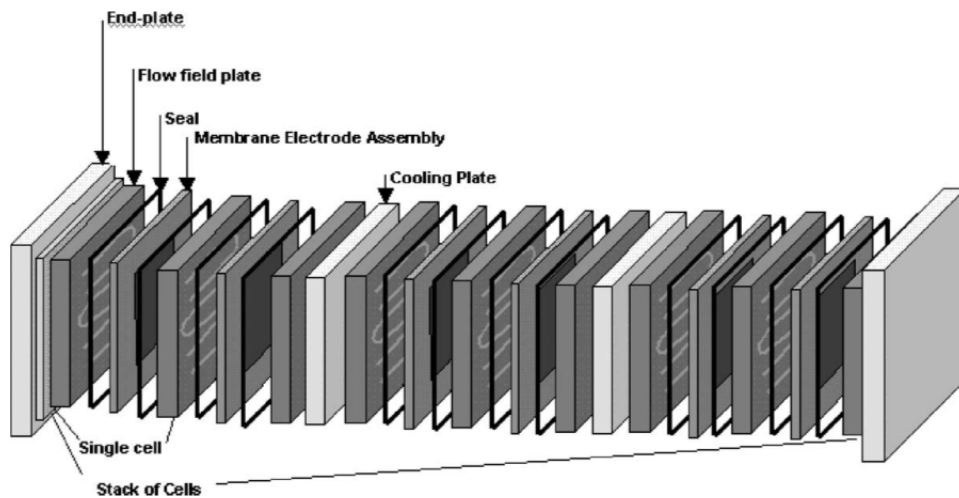


Figure 3.    PEM fuel cell system set up. From [6].

In a PEM fuel cell stack, in-between each cell are flow field plates; these plates serve multiple purposes. Structurally, they provide support for adjacent cells and separate the individual cells in the stack. Functionally, the flow-field plates help distribute fuel and oxidant within the cell, manage the water that was generated due to the reactions, and collect the current that is produced from the cell. In addition, if the PEM fuel cell does

4

not incorporate cooling plates with in the stack, the flow-field plates help manage heat generated from the reduction and oxidation reactions [6].

The purpose of the membrane-electrode assembly is to keep the steadily supplied fuel and oxidants separated, but allow the protons to pass through to facilitate the reduction and oxidation reactions so that electricity can be generated. It consists primarily of three sections. The first section consists of gas diffusion layers that ensure direct and uniform distribution of fuel and oxidant into the catalyst layers. The second consists of two dispersed catalyst layers that facilitate the oxidation and reduction of hydrogen and oxygen. These catalysts usually consist of platinum or a platinum alloy and will be discussed in greater detail later [6]. The final section is the membrane that acts like a "check valve" for the reduction and oxidation reactions.

The typical membrane material is a perfluorosulfonic acid (PFSA), and one commercial form, 'Nafion' currently dominates the industry. Nafion is a sulfonated tetrafouroethylene fluoropolymer-copolymer ($C_2F_4$–$C_7F_{13}O_2$–($SO_3H$)) [7]. The membrane is proton permeable allowing protons to pass freely while preventing electrons from crossing over and short circuiting the cell. This is because the substituent sulfate groups on the polymeric background act as cation-exchange sites.   As a result protons are able to conduct as ions move from one anionic sulfate group to another. With no alternative the electrons that are generated on the anode are then forced to flow to an external load there by creating a current and generate useable energy [5], [6].   It should be noted that Nafion, and similar materials, behave as a strong acid $pK_a$ ~ 6. This causes corrosion and other issues with internal components of the cell.

There are two distinct advantages of using PFSA products. The first is that the structure is strong and stable in the fuel cell's oxidative and reductive environments. In fact it is so resilient that a durability of 60,000 hours has been reported, which meets the DOE requirements for durability [3], [8]. The other advantage is the conductivity of protons. When operating at optimal conditions an achievable conductivity of 0.2 S/cm is viable. As a result cell resistance can be low as 0.05 $\Omega$ cm$^2$ for a 100 μm thick membrane. This low resistance means that there is only a 50 mV at A/cm$^2$ thus improving performance of the fuel cell [7].

5

## C.    TECHNOLOGICAL PROBLEMS WITH PEM FUEL CELLS

Despite the advantages of PFSA membranes there are several draw backs. First, the cost of the membrane, and related parts, is too high. Current production costs 25 μm thick PFSA membrane is approximately $250/m$^2$. In order to make fuel cell technology competitive, in terms of capital investment, with internal combustion the price would need to drop to about $10/m$^2$. This would result in fuel cell costs of $1.5/kW making it competitive with the current cost of standard automotive combustion engines [9]. The second is the requirement of additional support equipment, such as a hydration system. This adds additional cost, weight, space requirements, and complexity to the system making it less viable for commercial use in the automotive sector [8]. Finally, the most crippling disadvantage is the inherent temperature limitations.

At temperatures above 175$^o$C PFSA membranes decompose releasing toxic and corrosive gases. This imposes a safety risk during vehicle accidents, or manufacturing mishaps, thus limiting recycling options. Unfortunately this component is not biodegradable and requires to be disposed of in a landfill [10]. Besides the safety concerns, PFSA membranes proton conductivities change. The conductivity at an operating temperature is 60$^o$C is 10 times greater than 80$^o$C [11]. Furthermore, temperatures above 80$^o$C result in reduced material strength, membrane dehydration, decreased affinity for water, and parasitic losses through high fuel permeation [8].

It is desirable to operate at higher temperatures because fuel cell performance is increased, as well as durability, with elevated operating temperatures.   This is a result of increased reaction rates and reduced likelihood of electrode flooding. Most importantly it minimizes catalyst poisoning [11]. Catalyst poisoning is the direct result of impurities in the hydrogen and oxygen fuel supply, or contamination from parts in the assembly [12–16].

The biggest contributors to catalyst poisoning are impurities in the hydrogen and oxygen fuel resulting from the process used to create the fuel and from the presence of impurities in the environment. Currently the most common way to produce hydrogen is through the reformation of the hydrocarbons or oxygenated hydrocarbons from either

6

methane or methanol. During the reformation process byproducts such as CO, $CO_2$, $H_2S$, and sulfur organics are unavoidable [12–14]. Equally, the most practical and economical source for oxygen is air. Unfortunately, air also contains pollutants from automotive exhaust and industrial factories (e.g., nitrous, sulfur, and carbon oxides) will also undergo reactions. These unintended reactions cause negative effects to the fuel cell's performance [15].

   As the gases feed into the system they undergo oxidation and reduction reactions. Likewise, the impurities inside the gases undergo reactions as well. These reactions cause poisoning of catalysts sites by changing key properties such as hydrophobicity and hydrophilicity. As a result this modifies the proton transportation path and water management causing reduced catalyst activity [17]. This is particularly true for carbon dioxide because of its tendency to bond with the platinum sites in a catalyst. Often called CO poisoning, results in reduction of surface active sites for hydrogen adsorption and oxidation. This in turn reduces the overall performance and efficiency of the fuel cell.

   As mentioned earlier, the membrane-electrode assembly for a typical PEM fuel cell uses a platinum catalyst. The platinum catalyst is used to increase the rate of the reactions by providing an alternate reaction path with lower activation energy barrier [4]. Platinum is able to withstand the corrosive conditions in the acidic environment at the desired hydrogen potentials; however, it strongly absorbs CO. This process occurs with dissociate chemisorption and electro-oxidation reaction. Equations 4 through 7 illustrate this process.

$$H_2 + 2Pt \rightarrow 2Pt - H_{ads} \qquad (4)$$
$$2CO + Pt \rightarrow Pt - 2CO_{ads} \qquad (5)$$
$$2CO + 2Pt - H_{ads} \rightarrow 2Pt - 2CO_{ads} + H_2 \qquad (6)$$
$$2Pt - H_{ads} \rightarrow 2Pt + 2H^+ + 2e^- \qquad (7)$$
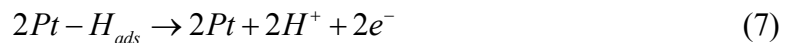
   Reaction 4 is slow compared to the reaction 7, as it requires two adjacent platinum sites. The adsorption of CO (reactions 5 and 6) occur at bare platinum and platinum hydride sites. It is hypothesized that this mechanism requires linear-absorbed CO species involving one adsorption site per CO molecule. Likewise, a bridge-bonded CO species requires two nearby platinum surface sites. As a result this can lead to a

7

configuration that causes the CO molecule block more than one hydrogen site [18], [19]. This then causes $H_2$-oxidation rate to reduce thereby dropping fuel cell performance. CO poising is strongly affected by concentration of the gas, the exposure time, and temperature. Figures 4 through 6 show the performance drop for a fuel cell as it is poisoned from carbon oxides [20–22].
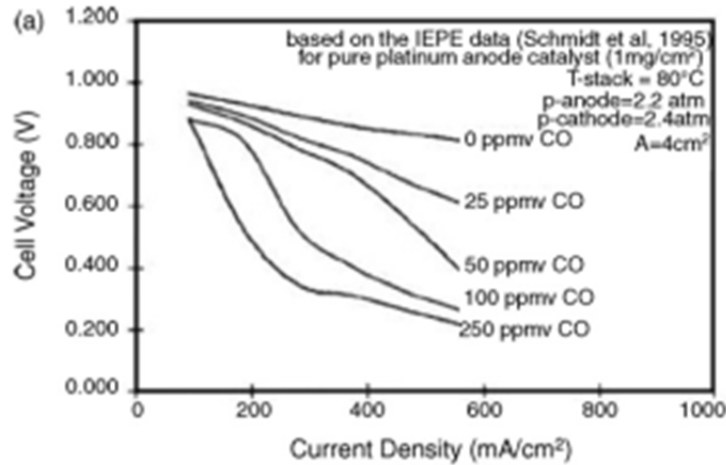


Figure 4.    Cell Voltage vs. Current Density data for experiments involving concentration. From [20].
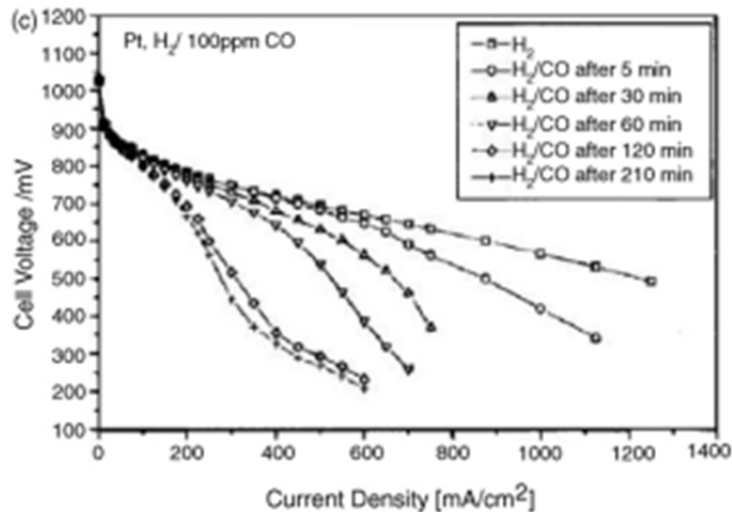


Figure 5.    Cell Voltage vs. Current Density data for experiments involving exposure time. From [21].

8
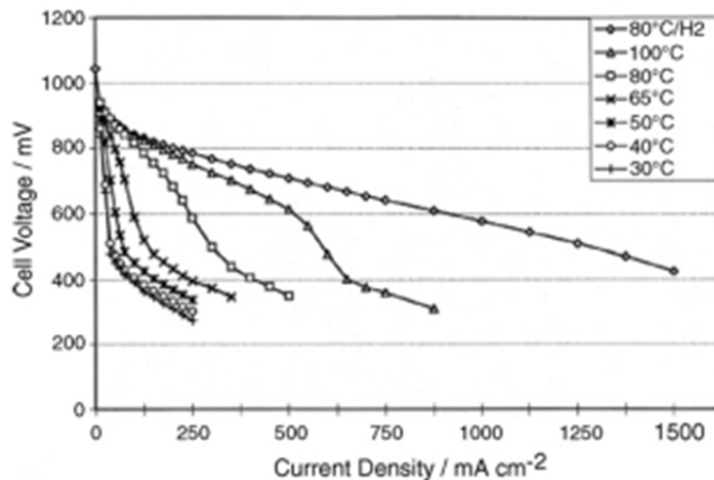
Figure 6.    Cell Voltage vs. Current Density data for experiments involving temperature.
From [22].

To mitigate CO poising of the platinum catalyst efforts have been made to alloy with other materials. This alloying process requires the use of one or two elements to block the adsorption of CO but allow hydrogen adsorption. Selection of these materials is based on the resilience of the material on the harsh environment of the cell, the electrical conductivity, and high surface area. Table 1 lists relative research into using different alloying elements to combat CO poisoning with varying degrees of success [23–33].

| Pt-Mo | Pt-Ni | Pt-V | Pt-Ru-Mo | Pt-Ru-Ni | Pt-Ru-V |
|-------|-------|------|----------|----------|---------|
| Pt-Nb | Pt-Fe | Pt-Zr | Pt-Ru-Nb | Pt-Ru-Fe | Pt-Ru-Zr |
| Pt-Ta | Pt-Cr | Pt-Pd | Pt-Ru-Ta | Pt-Ru-cr | Pt-Ru-Pd |
| Pt-Sn | Pt-Ti | Pt-Os | Pt-Ru-Sn | Pt-Ru-Ti | Pt-Ru-Os |
| Pt-Co | Pt-Mn | Pt-Rh | Pt-Ru-Co | Pt-Ru-Mn | Pt-Ru-Rh |

Table 1.    This is a listing of different catalysts used to mitigate CO poisoning effects
in fuel cells. After [23–33].

9

Another major problem with current generation catalysts identified by DOE is the poor durability of current generation anode (oxygen reduction) catalysts [3]. Virtually all catalysts for the anode are generated on carbon, and it is clear that the metal particles rather rapidly agglomerate during operation. Other support materials (e.g., molybdenum nitrides) for catalysts are currently being researched in order to solve the durability issues. While conducting research into molybdenum nitrides, scientists at Los Alamos National Lab (LANL) recently discovered findings that suggest a novel means to overcome this persistent durability issue. They are working on a highly conductive, ceramic support to replace carbon. Specifically, they focused on the use of molybdenum carbide ($Mo_2C$) support material for platinum. Figure 7 displays the recent test data of $Mo_2C$ synthesized by newly developed routes compared to commercial platinum and titanium oxide in a traditional support material. It can be seen that the $Mo_2C$ can be synthesized in a manner that is far superior to other support catalysts in terms of durability. Moreover (not shown) on a per gram platinum basis this support catalyst was found to outperform, even at the start, the best commercial carbon support based anode catalyst [34].
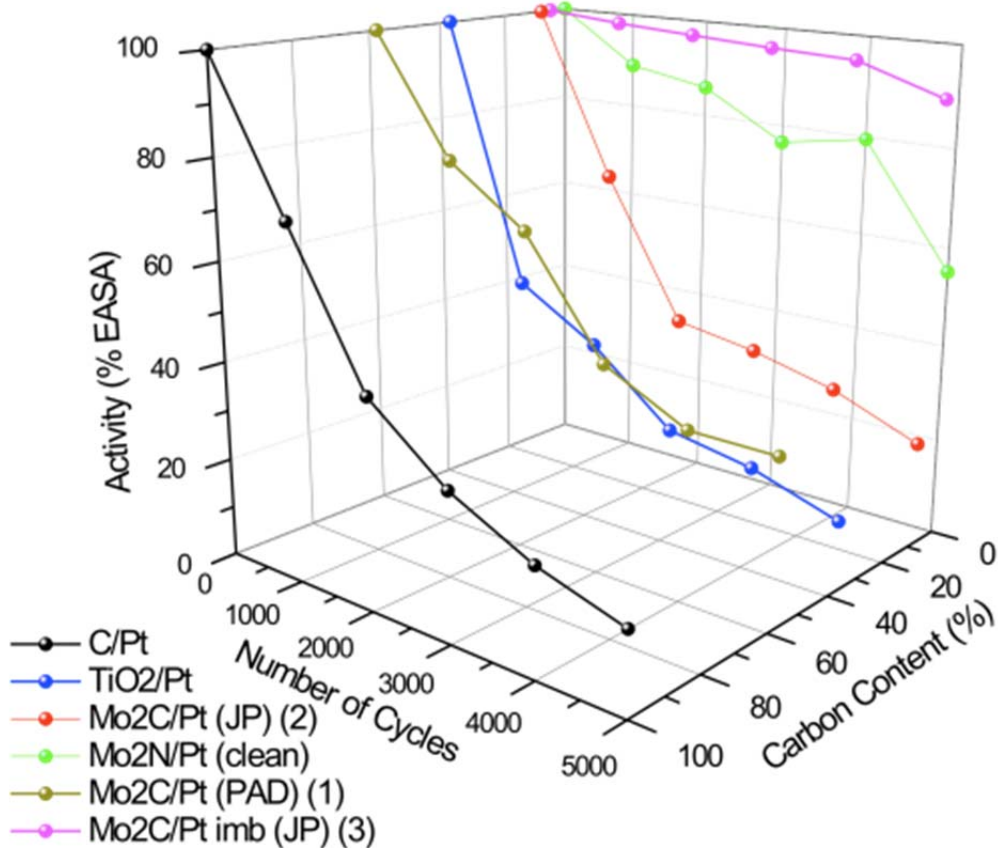
Figure 7.   Durability testing of half-cell using Mo₂C Platinum catalyst. From [34].

## D.   USING PLASMAS TO MAKE CATALYSTS

Conventionally catalysts have been synthesized using incipient wetness and other variants of, "wet impregnation." The most common procedure is to add an aqueous solution containing a dissolved metal precursor salt (e.g., platinum chloride) to a high surface area refractory oxide (e.g., alumina). The liquid is added in an amount just sufficient to fill the pores of the catalyst support via capillary action, hence 'incipient wetness'. No liquid water should be present on the powder. Next the catalyst is dried and calcined in order to drive off volatile components within the solution. This process leaves metal or metal oxide particles deposited as small particles (generally less than 100 nm) deposited on the surface of the refractory oxide. There are some limitations with this method because maximum loading is limited by the solubility of the precursor in the solution. The concentration profile of the metal particles within the refractory oxide

11

support depends on the mass transfer conditions within the pores during the impregnation and drying. In addition this process takes time, generally hours [35].

A relatively new method of synthesizing catalysts uses plasma processing. Plasma processing has been used extensively in the commercial industry to make circuits, transistors, resistors, capacitors, VLSI, displays, solar cells, and etc. [36–39], but until recently it had not been used for creating catalysts or other particulate structures. Example of catalysts synthesis use an atmospheric-pressure microwave system, aerosol-through-plasma (ATP) technique, is found in the literature [40], [41]. As reviewed in detail elsewhere, other variants on the ATP process have been employed to make numerous particulate materials including nano-metal particles, nano oxide particles, carbon nanotubes, graphene, etc. [42]

In the ATP process for the production of supported metal catalysts, the first step is to create low solid density aerosols consisting of mixtures in the targeted final catalyst ratio (e.g., metal particles and refractory oxide powders by one weight percent of metal). The aerosol is then passed through a plasma region where gas temperature is generally in excess of 3000 K.   Generally, the precursors in the aerosol are exposed to the plasma for less than a second, but that is sufficient for transformation due to the high temperature and unique chemistry [43], [44].

The mechanism of transformation from metal particles and refractory oxide powder aerosol to supported metal catalysts appears to be simple. In the hot zone of the plasma the metal precursor is atomized, but the refractory support is only marginally impacted. This is because the melting temperature of the refractory is typically much greater than the melting and boiling points for the metal. As the aerosol passes out of the hot zone into the much cooler 'afterglow' the atomic constituents of the metal precursor, that is metal atoms, condense on the refractory oxide surface. The cooling in the afterglow is very fast, thus preventing significant agglomeration of metal atoms on the refractory oxide surface [40], [41], and [45].

After undergoing the transformation the particles are collected downstream via a filter paper, or being scraped off surfaces exposed to the aerosol gas. The final result of

this process is a multi-scale sized material. The active metals are generally in the nano scale, while the support materials are not [40–42].

This process has many advantages relative to conventional methods. It is able to drive down cost by better dispersion of the active material (e.g., Platinum). That is, it has been empirically demonstrated that the A-T-P process yields smaller, more thermally stable particles than those produced using incipient wetness. The greater durability of A-T-P produced particles suggests they bind more strongly to the support, generally alumina, than metal particles produced using incipient wetness. Furthermore, the overall process is relatively simple, requiring the mixing of precursors, generation of an aerosol gas, and collecting the products after they have passed through the plasma [40], [41].

Various research and experiments have been carried out to determine if ATP produced catalysts produce compositions and properties that are comparable to conventionally made catalysts. One such work used lead and lead-silver catalysts for selectively hydrogenation acetylene in a stream of primly ethylene. The study's purpose was not to determine the catalytic activity but the selectivity of the final product. The results showed that the ATP generated catalysts were superior to the commercially synthesized catalysts [45].

Other published research work studied the modification of catalysts in plasmas. This process used catalysts and ceramics, or carbon, to make precursors. These precursors were then processed using the ATP method under different operating conditions. These conditions included operating slightly below atmosphere (less than 1 tort), plasma gases, and power. This resulted in some improvements to the catalyst performance in activity and selectivity [46–49].

## E. THESIS OBJECTIVE

The objectives for this thesis research are as follows:

- To develop protocols for making small, high-surface area Molybdenum nitrides or carbides using the ATP method

- Fully characterize the structure, microstructure, and surface area of the synthesized material

- To generate enough material to test the performance and stability, appropriately loaded with Platinum catalyst particles, in an operational fuel cell.

## F. HYPOTHESIS

The methods used in this research will to be able to synthesize a high surface, highly conductive molybdenum nitride or carbide loaded with platinum to form a catalyst, and this catalyst will be superior to that of conventional prepared platinum on carbon catalysts in a fuel cell environment.

# II.   EXPERIMENTAL METHODS

## A.   ATP SETUP AND OVERVIEW

For this study a relatively new method for making catalysts was implemented. It employs the use of microwave energy to produce plasma discharge and applying that discharge to an aerosol containing precursor species. This ATP method leads to the decomposition of the precursor species to form an "atom and molecular fragment soup," due to extreme heating. The "fragment soup," can reorganize in the plasma afterglow to form support metal particles and hence a catalyst.

Figure 8 is a picture of the system used for this research, and Figure 9 is a block diagram of the system. A power supply (A) provides electrical power to a magnetron (B) which is used to generate the microwave energy. A series of wave guides (C) direct the energy forward while a stub tuner (D) creates a focus point. At this point plasma is generated (E). A gas (F) passes through a flask (G) containing a precursor in order to generate an aerosol. This aerosol is carried up through a quartz tube. Gas for the plasma (H) is supplied to the torch (I), and this is where the precursor is exposed to the plasma. The final product deposits either on the chimney (J) or on a filter (k). Finally a pump (L) removes the exhaust gases out of the room.
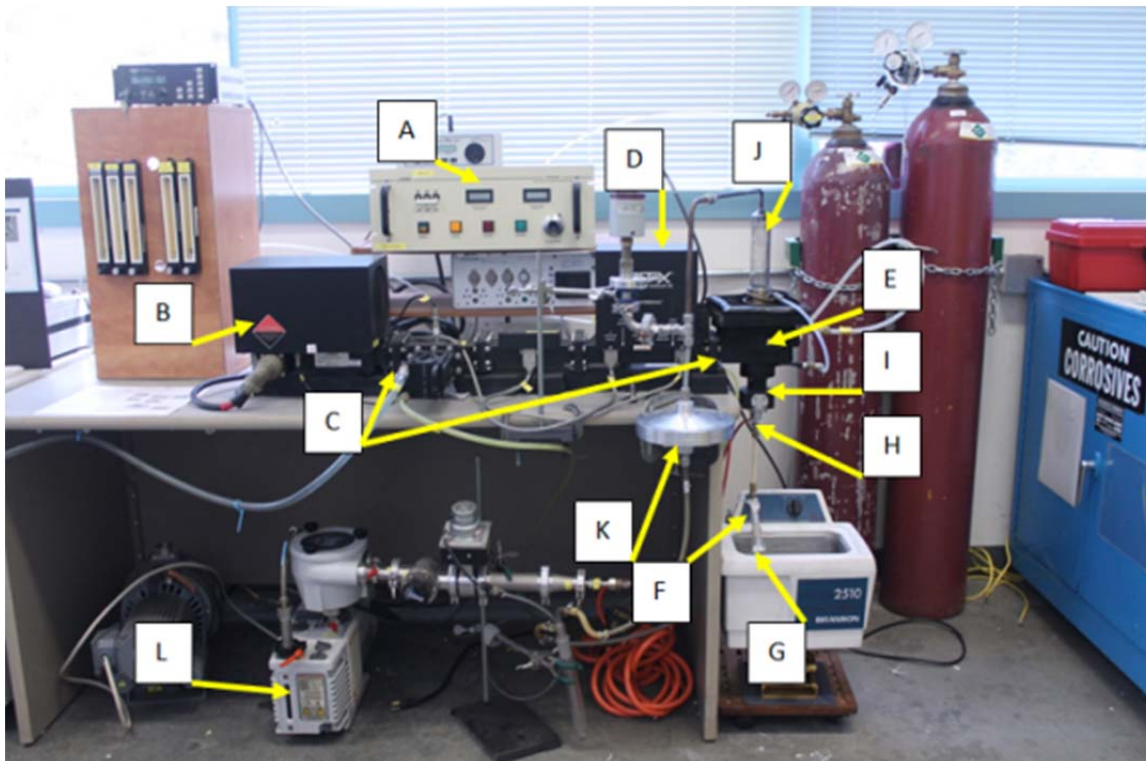
Figure 8.　A picture of the general ATP system set up.
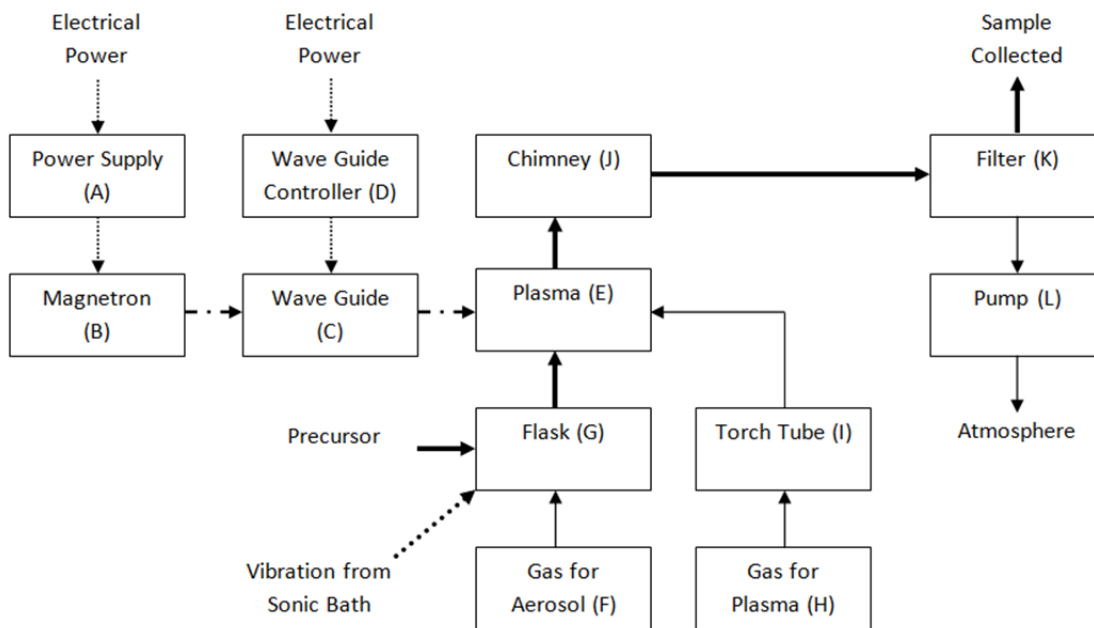


Figure 9.　A detailed block diagram showing the ATP method.

As previously mentioned, plasmas were generated using a magnetron. A magnetron produces microwave energy by the use of high voltage and a combination of electric and magnetic fields. Electrical current is sent to a cathode, which produces heat. This heat increases molecular activity causing the emission of electrons between the cathode and anode. Since the cathode and the electrons have a negative charge the electrons start to move toward the anode, which is positively charged. An antenna is used to guide the electrons toward the anode. As the electrons move at a high rate of speed they encounter a magnetic field and impart a force on the electrons. The force balance of electric charge and the magnetic field cause the electrons to circulate at a specific frequency, the so-called plasma frequency. It is this frequency (2.45 GHz in the present system) that determines the wave guide dimensions, and hence the size of the quartz torch. In turn, the size of the quartz torch determines the rate at which material can be processed using the ATP approach. Furthermore, for atmospheric pressure systems microwave permits plasma production from a broader array of gases including oxygen and nitrogen, whereas radio frequency (RF) is limited to Argon with low percentage of other gases. As the electrons travel in a circular orbit microwave energy is released. Figure 10 shows the power supply and magnetron used for this setup. The total amount of microwave energy is regulated by the power supply by changing the input power. For all experiments the input power was set to 900 watts.



Figure 10.   On the left is the power supply and on the right is the magnetron.

Once the microwave energy is produced it travels through a wave guide toward the torch chamber. Gas, from below, passes through a vertically oriented, ~1" OD cylindrical quartz tube ("torch") that fits through a special cavity near that end of the wave guide furthest from the magnetron. A three stub tuner is used to focus the microwave energy on the torch to maximize the amount of energy used to generate the plasma. The three stub tune works by changing the impedance of the system. Stubs are raised and lowered to introduce a shunt capacitance resistance to the system. When the stubs are perfectly, or near perfectly, aligned the load of the impedance is matched to the intrinsic impedance of the wave guide, and as a result the maximum power is transferred to the plasma. This has the added benefit of protecting the magnetron from energy that could bounce back and cause an overload. Figure 11 is a picture of the wave guide, and stub controller used.
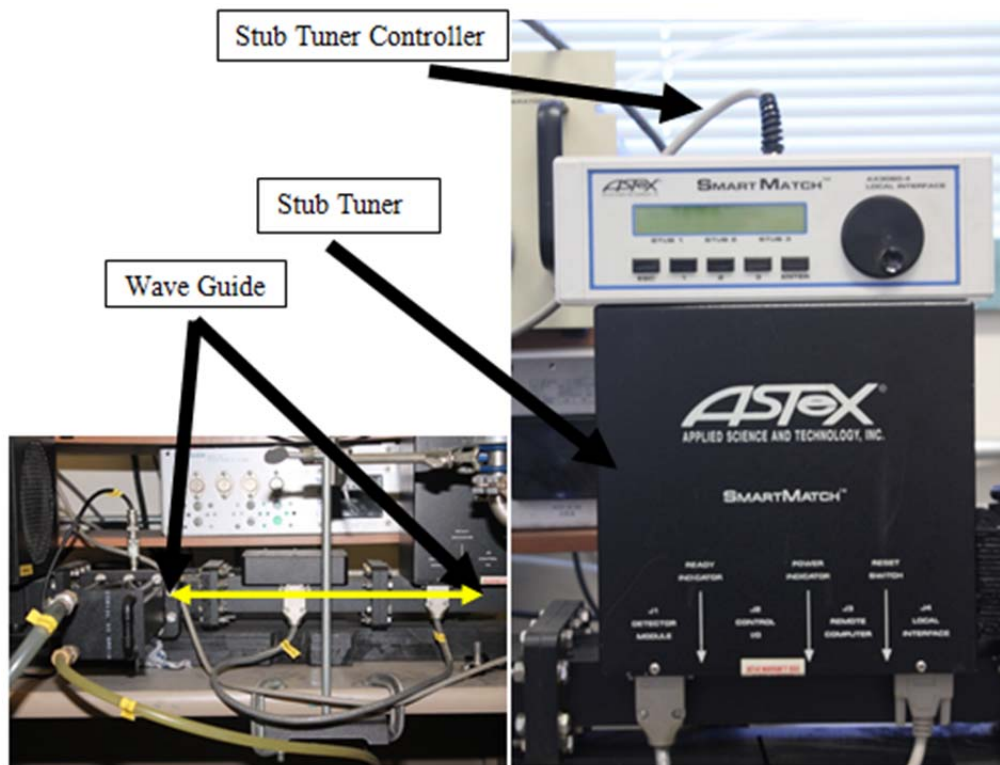


Figure 11.   These are pictures of the wave guide, stub controller, and the stub tuner.

Precursor powder, located in a flask just below the waveguide is turned into an aerosol by two processes: I) the aerosol gas is directed through a small diameter tube (1/16″) to impinge on the solid precursor, and ii) the entire beaker is placed in a sonic bath. The water in the sonic bath is there to vibrate the solid precursor in order to facilitate the formation of an aerosol. This set up can be seen in Figure 12.



Figure 12.   Picture of a sample loaded into the sonic bath.

The aerosol is then carried upward through a 1′ long OD quartz torch that terminates inside the wave guide at the microwave focus point. At this focus point all the energy of the microwave, focused using a three-stub tuner, heats the aerosol to a temperature of 2000–3000K. This forces the precursor to vaporize and break down into atoms and/or molecular fragments. Figure 13 is a cut away view of the process that was described above. When the atoms and fragments exit the plasma stream and enter the chimney they quickly cool back down to room temperature. At this point the atoms recombine rapidly and form new species. For this work, precursors and conditions were selected to favor a "restructuring" in the form of catalysts, that is very small (ca. order of 1nm) platinum metal particles on finely divided and high surface area $Mo_2C$. The conditions were not "engineered," but rather selected on the basis of empirical studies of similar systems. Figure 14 is a picture of the chimney when the plasma torch is running. The final products deposit either on the chimney or downstream on a 0.1 μm filter (Figure 15).
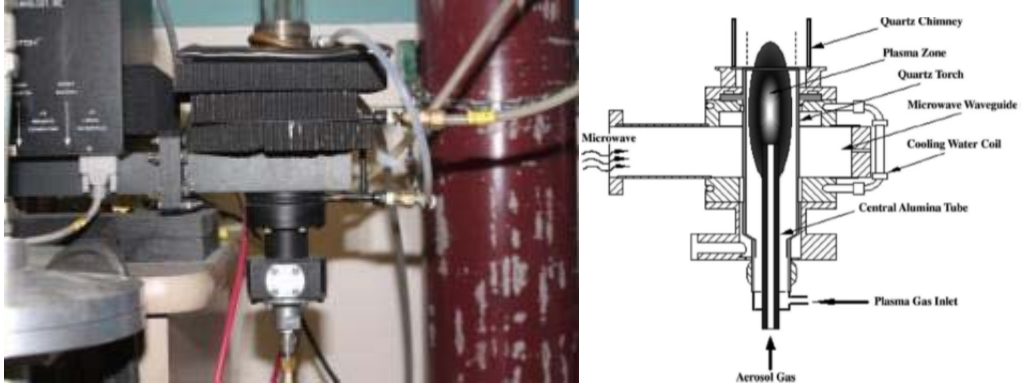
Figure 13.  This figure shows a cut away view of the plasma chamber. From [50].
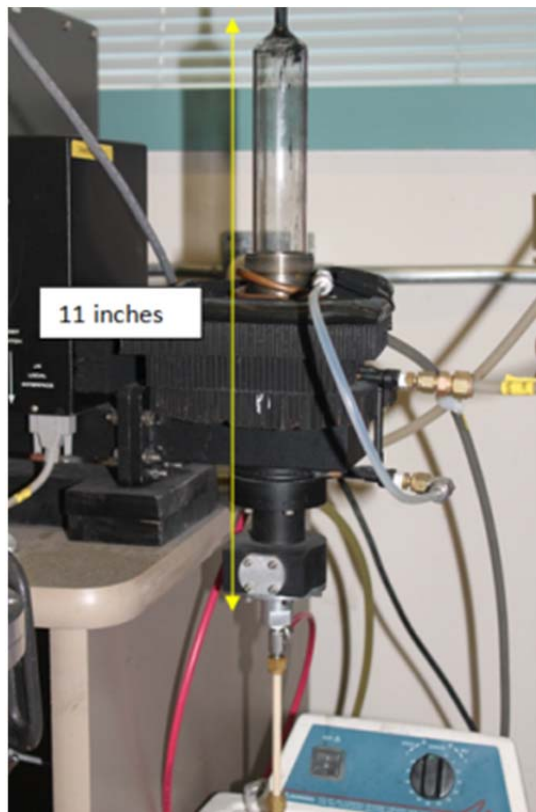


Figure 14.  This is a figure of the plasma system operating with the chimney.
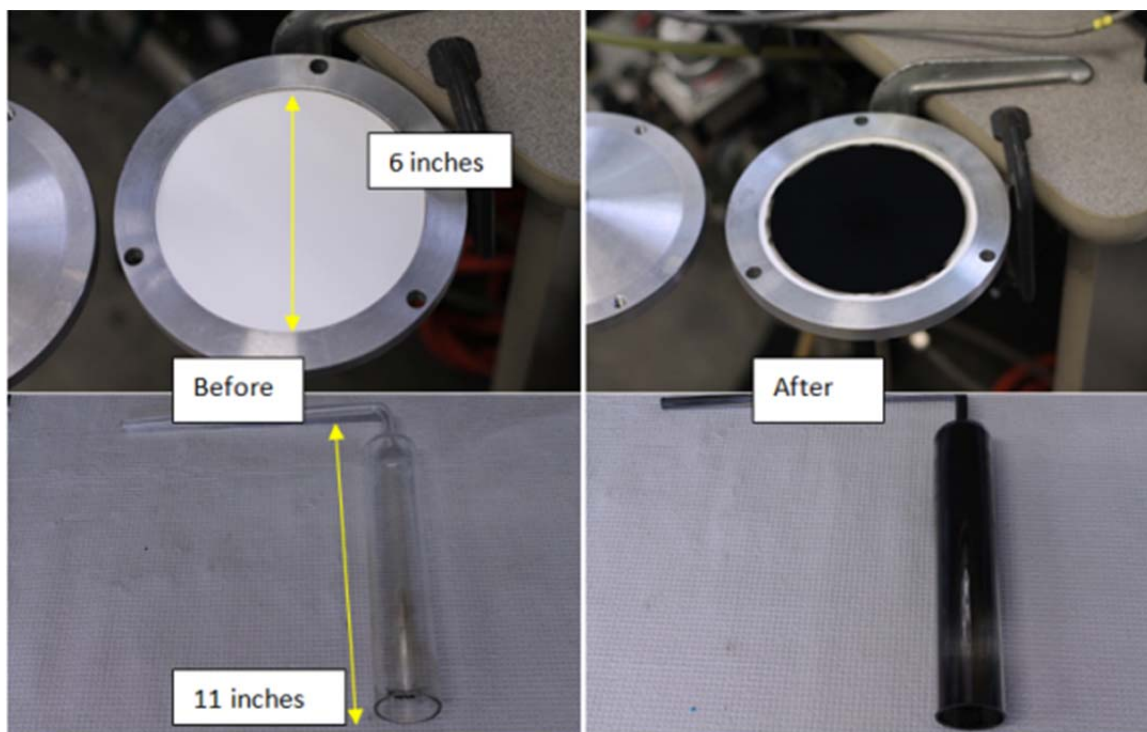
Figure 15.   Before and after pictures of the filter and chimney.

Indeed there are four main steps in the ATP process for preparing catalysts, and this general approach is broadly outlined in earlier literature [40]. The details of the procedure employed in the current research differ significantly from that employed earlier; hence, the protocol used in this work is described in detail below. The general ATP procedure used in the current work is a series of four steps. These steps are 1) preparing the precursor mixture, 2) loading the mixture into the aerosol container and preparing the aerosol system, 3) selecting the operation conditions for the plasma and initiating the plasma, 4) passing the aerosol through the plasma the plasma system and collecting the product.

## B.     PRECURSOR PREPARATION

A variety of precursors were used in an effort to synthesize molybdenum nitride and eventually molybdenum carbonate (the latter being of interest given previous reports on its application in the field). Base precursors that had a substantial amount of molybdenum were used. These were ammonium molybdate tetrahydrate ($(NH_4)_6Mo_7O_{24}$

4H$_2$O) and ammonium molybdate ((NH$_4$)$_2$MoO$_4$). Using a mortar the precursor was crushed into a fine powder. In some cases additives were added to facilitate the development of a carbide or nitride catalyst. The powder was then placed in a vial and dried using nitrogen gas for one hour. Figure 16 is demonstration of this. Table 2 is a listing of the different types of precursors used with the additives added based on weight percent. For example for Method 3 if there was 1 gram of (NH$_4$)$_2$MoO$_4$ then 1 gram of Urea was added. In order to properly form an aerosol no more than 3 grams of precursor was loaded into the vial.



Figure 16. This figure shows the process used to prepare a precursor from left to right. It involves measuring the precursors, crushing them into a fine powder, and then drying them using nitrogen gas.

| Mixture | Precursors | % Weight | Additive | % Weight |
|---------|-----------|----------|----------|----------|
| 1 | (NH$_4$)$_6$Mo$_7$O$_{24}$ 4H$_2$O | 100 | None | n/a |
| 2 | (NH$_4$)$_2$MoO$_4$ | 100 | None | n/a |
| 3 | (NH$_4$)$_2$MoO$_4$ | 50 | Urea | 50 |
| 4 | (NH$_4$)$_2$MoO$_4$ | 48.5 | Urea | 48.5 |

Note: Method 4 added %5 Pt using Tetra amine Platinum Nitrate

Table 2. A listing of the different types of precursors based on weight percentage used.

Each "ingredient" of the precursor mix has an intended role in the product. Specifically i) ammonia molybdate is intended to decompose releasing molybdenum to form metal particles, or recombine with the presence of carbon atoms from other precursors (Mo$_2$C), ii) Urea is intended to release reducing species to remove oxygen and

to produce carbon for MoN or Mo$_2$C, iii) ethylene could also further serve as a source of carbon atoms and reducing species, iv) tetramine platinum nitrate is intended to yield platinum atoms to from metal platinum particles and reducing molecular "fragments" to help remove oxygen.

Once the precursor was fully prepared the vial was loaded into the loaded into the plasma torch by sealing it with a rubber seal. Two 1/16″ tubes were used to penetrate the rubber seal to provide gas for the aerosol process and the uptake line to the plasma torch. It was then placed into an ultrasonic bath where the water level was adjusted such that it did not touch the seal. The ultrasonic bath was then turned on and all connections were checked for any water and gas leakage. Figure 17 is a demonstration of the process mentioned above.



Figure 17.   This is a depiction of loading the sample into the system and adjusting the water level of the sonic bath.

## C.    PROCESSING AND COLLECTION OF PRODUCT

Prior to each start up gases for plasma and the aerosol were selected. The flow rates for the selected gases were controlled by using Matheson 605, 604 603, and E100 (B) series flow meters (Figure 18). Table 3 is a listing of the types of gases used, what the purpose of the gas was, and the type of flow meter used to regulate the gas. In addition, the table lists what precursors were used during that experiment.



Figure 18.   This is a picture of the flow meters used for the system.

| Flow Meter | Gases Used | Location | Precursors used |
|---|---|---|---|
| 603 | Ultra High Purity Argon | For Aerosol Gas | Mixtures: 1,2,3,4 |
| 604 | Ultra High Purity Argon Gas | For Plasma Gas | Mixtures: 1,2,3,4 |
| 604 | Nitrogen Gas | For Aerosol Gas | Mixtures: 1 |
| 605 | Nitrogen Gas | For Plasma Gas | Mixtures: 1 |
| E(100)B | Argon Gas with 2% Hydrogen | For Aerosol Gas | Mixtures 2,3,4 |
| E(100)B | Ethylene | For Aerosol Gas | Mixtures 2,3,4 |

Table 3.    This is a table that shows what gases were used and with what precursors.

Startup for all experiments used argon gas for the plasma. The argon gas was set to a flow rate of 0.309 g/min with the chimney removed. The magnetron was then turned on and microwave energy was produced. A metallic probe was used to strike an arc in order to start the ionization of the gas. This was accomplished by lowering the probe into the torch chamber. Figure 19 illustrates this process starting left, where a metal tip on an electrically insulted glass rod is lowered into the plasma torch at the center of the microwave wave guide. Once the metal tip reaches the center of the wave guide a loud "pop" is heard resulting in ignition (center), and the plasma is ignited and is easily visible (right).



Figure 19.   This figure shows the process to start the plasma.

Once the gas ionized to produce plasma the chimney is reattached and the system is sealed from atmosphere. The system was operated and maintained 10 torr above atmosphere.   A MKS 600 series pressure controller controlled exhaust gas emissions and a pump was used to force the exhaust gases into a hood. Here the gas was vented to atmosphere. This was to insure that system pressure stayed above atmosphere to prevent oxygen from entering the plasma chamber, and create a safe environment for the operator. Figure 20 shows the different instruments that were mentioned and the chimney when the system is fully sealed.

Figure 20.   Top left shows the chimney when it is attached, the top right shows the MKS
controller used to regulate system pressure, and the bottom shows the pump
and control valve used to exhaust the gases.


Once system pressure was stabilized to 10 torr above atmosphere the sonic bath
was turned on and aerosol gas was then slowly opened. The aerosol gas was opened
slowly so that the system pressure did not exceed 15 torr above atmosphere and the
reflected power did not exceed 40 watts. This was to prevent precursor from moving too
rapidly through the plasma stream so that it gets sufficiently vaporized. In addition, it
provided a factor of safety for the operator and the equipment. For some experiments two
gases were used for the aerosol. A Tee fitting (Figure 21) was used downstream of the
flow meters to combine the two different gases into one supply line for the aerosol gas.

Figure 21.  This picture shows the Tee used to combine two different gases
to be used for making the aerosol.

The flow rates for the aerosol and plasma gases varied from experiment to experiment. Once the system was operating the aerosol and plasma gases were adjusted to produce a steady stream of precursor passing through the plasma. This was determined by monitoring the products coming up through the chimney. For experiments that involved the use of two aerosol gases only the argon gas flow was adjusted. Figure 22 is a picture of a running experiment with the proper flow rates.   Table 4 is a complete listing of all experimental runs with the flow rates and precursors used.
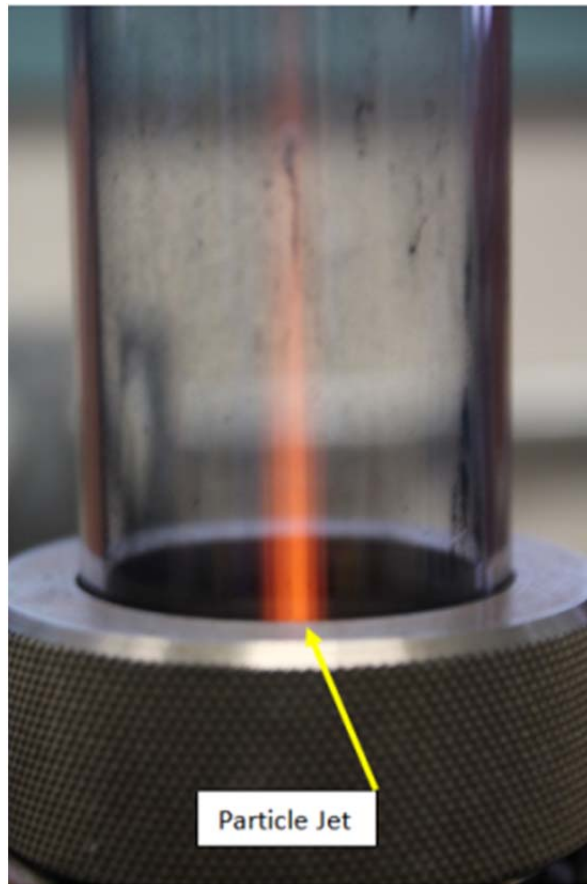
Figure 22.   This is a figure of a steady stream of particles flowing through the plasma. It is estimated that a small fraction of 1% of the plasma volume consists of aerosol solids.

| Experiment | Precursor Mixture | Gas Used | Flow Rate (g/min) | | Additional Notes |
|---|---|---|---|---|---|
| 1 | 1.5 g of $(NH_4)_6Mo_7O_{24}$ | Ultra High Purity (UHP) Argon | Aerosol: | 0.069 | - |
| | | | Plasma: | 0.457 | |
| 2 | Same as above | Nitrogen Gas | Aerosol: | 0.090 | - |
| | | | Plasma: | 0.511 | |
| 3 | 1.5 g $(NH_4)_2MoO_4$ | UHP Argon | Aerosol: | 0.131 | - |
| | | | Plasma: | 0.521 | |
| 4 | Same as above | UHP Argon | Aerosol: | 0.131 | Argon gas with 2% $H_2$ was supplied at 0.115 g/min to the aerosol line. |
| | | | Plasma: | 0.309 | |
| 5 | Same as above | UHP Argon | Aerosol: | 0.131 | Ethylene gas was supplied at 0.075 g/min to the aerosol line. |
| | | | Plasma: | 0.416 | |
| 6 | 0.75 g $(NH_4)_2MoO_4$ + 0.75 g Urea | UHP Argon | Aerosol: | 0.131 | - |
| | | | Plasma: | 0.521 | |
| 7 | Same as above | UHP Argon | Aerosol: | 0.131 | Argon gas with 2% $H_2$ was supplied at 0.115 g/min to the aerosol line. |
| | | | Plasma: | 0.309 | |
| 8 | Same as above | UHP Argon | Aerosol: | 0.131 | Ethylene gas was supplied at 0.075 g/min to the aerosol line. |
| | | | Plasma: | 0.416 | |
| 9 | Same as above | UHP Argon | Aerosol: | 0.131 | Ethylene gas was supplied at 0.1 g/min to the aerosol line. |
| | | | Plasma: | 0.416 | |
| 10 | Same as above | UHP Argon | Aerosol: | 0.131 | Ethylene gas was supplied at 0.128 g/min to the aerosol line. |
| | | | Plasma: | 0.416 | |
| 11 | 0.75 g $(NH_4)_2MoO_4$ + 0.75 g Urea + 0.04 g $H_{12}N_6O_6Pt$ | UHP Argon | Aerosol: | 0.131 | Same as above |
| | | | Plasma: | 0.416 | |

Table 4.    This is a summary of all the experiments along with the different gas and precursor mixtures used.

For experiments involving nitrogen the process was first started with the use of argon plasma. After achieving a system pressure 10 torr above atmosphere nitrogen gas was slowly opened and the argon plasma gas was slowly closed. This was done in a manner such that the system pressure did not exceed 15 torr and the reflected power did not exceed 60 reflected watts. Once the system was stabilized with nitrogen plasma, the sonic bath was turned on and the supply line for the aerosol gas was opened. Once the experiment was concluded the process was conducted in reverse so that the system was shut down using argon plasma.

Experiments operated under these conditions for 45 minutes; afterwards the machine was turned off. This was accomplished by slowly tuning off the aerosol gas so that the system pressure remained above 5 torr and that reflected power did not exceed 40 watts. The sonic bath was then turned off and the power to the magnetron set to the off state. The power supply was allowed to cool for 15 minutes before complete shutdown. It is important to note that experiments involving nitrogen gas the system was only operated for no more than 15 minutes. This was due to the fact that nitrogen plasma is much hotter than argon plasma and as a consequence increases the risk of damaging the equipment.

Once the machine was shut down the deposits were collected off the chimney and the filter. The filter casing was opened and the filter membrane removed. Figure 23 is a picture of the particles being collected from the filter so that it can be weighed, cataloged, and examined. The deposits from the chimney were collected in a similar manner by holding the chimney upside down and scraping the wall. Once all the deposits were removed from the wall of the chimney it was flipped back over. The particles would fall onto a wax paper for collection. Figure 24 illustrates this process.
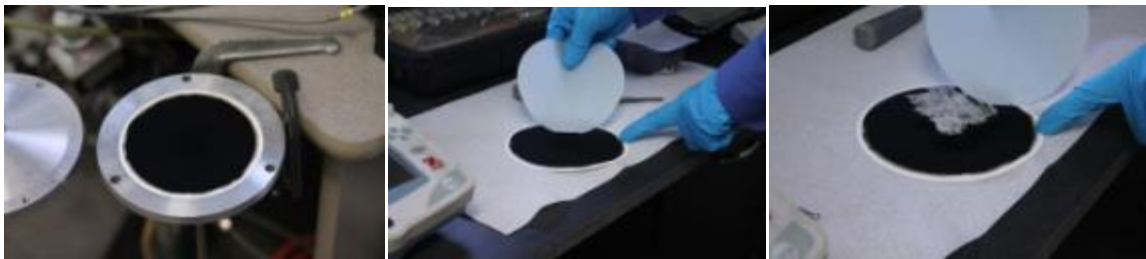


Figure 23.   This shows the samples being collected from the filter.



Figure 24.   This shows the samples being collected from the chimney.

# III. CHARACTERIZATION

## A. X-RAY DIFFRACTION

### 1. Purpose

X-ray Diffraction (XRD) was conducted on all samples in order to determine the existing phases based off a diffraction pattern. These diffraction patterns help identify the crystal phases present, thus only giving semi-quantitative analysis. This is due to the fact that diffraction patterns are dependent on how the elements are bonded together, the crystallographic structure of the material, what types of elements and the amount of elements present. As the name implies X-rays are used to generate a diffraction pattern. The X-rays are generated using a cathode and an anode operated at a large potential difference (e.g., 10 kV) [52].

The cathode and anode are contained in a lamp with beryllium windows which allow the X-rays to pass through, but allows the lamp to maintain vacuum. Beryllium's microstructure is uniquely suited for this because it has a minimum impact on the X-rays. A shutter is used to control the exposure. When the shutter is open it shines a beam of X-rays onto the sample [52].

When the shutter is opened and the beam of X-rays shines onto a sample the X-rays interact with the samples crystallographic structure. Depending on the crystalline planes present within the sample a pattern is formed. This can be related to Bragg's Law which gives the angles for coherent and incoherent scattering from a crystal lattice. The governing equation for this law is $n\lambda = 2d\sin(\theta)$ where $n$ is an integer, $\lambda$ is the wave length of the X-rays, $d$ is the spacing between planes in the crystal lattice, and $\theta$ is the Bragg angle. The Bragg angle is defined as the angle as between the source of the incident wave and the scattering planes [B].

Due to system set up and geometry it is necessary to mention that the XRD uses an angle called $2\theta$. This is due to the geometry between the shutter, the sample holder, and the X-ray detector. In particular the movement between the detector and the tray sample holder rotate in such a manner that the angle is doubled. The XRD analyzer

controls the movement of the x-ray detector while recording the intensity (known as counts) produced from the scattering at each angle. The counts vary as a function $d$ (spacing between planes in the crystal lattice), thus resulting in a pattern. This pattern can then be compared to a library of known patterns in order to determine the crystalline structures present. Furthermore the count peaks and the width of the peak can be used to roughly calculate the particle size [51].

For the purpose of this study the XRD was to characterize the product that was produced via the ATP method. Since the composition of the precursors and gases are known this helps isolate possible phases in the final catalyst based on the elements present. For example the method to make the final catalyst via ATP method used ammonium molybdate, tetramine platinum nitrate, ethylene gas, argon gas, and urea. This means that the only elements that should be present are oxygen, hydrogen, carbon, nitrogen, platinum, and molybdenum. This diffraction pattern can be compared to a library of known diffraction patterns that contain those elements. Due to the nature of the ATP process it is very likely that a mix of phases can be present [42].

### 2. Testing Parameters

The XRD analyzer used for this study was the Phillips PW1830 Diffractometer. This system has three primary parts: the lamp, the goniometer, and the X-ray detector. The lamp contains a tungsten cathode and a copper anode under a vacuum. As mentioned before this is the source for the X-rays. The goniometer is what holds the sample, and the X-ray detector is free to rotate around the goniometer to detect X-rays. Figure 25 is a picture of the system and setup of the Phillips PW1830 Diffractometer.

Figure 25.   This is a picture of the Philips PW1830 Diffractometer.

This particular XRD is designed to operate at 35 kV and 30 mA. The lamp is designed to generate electromagnetic energies from 200 eV to 1 MeV. The copper anode produces Cu Kα X-ray radiation that has energy of 8.04 KeV, and a wave length of 1.5418 Å. The X-ray detector is allowed to rotate from 0 to 90 degrees at a rate of 2 degrees per second.

All XRD scans were prepared by taking a small amount of product and onto a silicon disc sample holder. No bonding agent was used to hold the sample onto the tray. A silicon disc sample holder was used due to its favorable phase characteristics. The X-rays diffract parallel to the surface of the disc. This prevents the X-ray detector from detecting the X-rays that are interacting with the disc, but allows for better detection of small samples. The scan settings were set to 25° to 85° in step increments of 0.02°, and strict compliance with NPS operating procedures was followed.

## B.    SCANNING ELECTRON MICROSCOPE

### 1.    Purpose

The Scanning Electron Microscope (SEM) was used to capture high-magnification images of the catalysts with excellent depth of field. These images were to ascertain the particle size and consistency in order for further characterization. The SEM is able to accomplish this by the use of electrons instead of light to produce images. The electrons are generated similar to a cathode ray tube in older televisions. A cathode is heated up and electrons are generated. These electrons travel away from the cathode and a series of electromagnetic lenses focus the electrons in a beam toward the sample [52]

When the electrons hit the sample two reactions occur. The first reaction occurs due to the fact that some electrons will collide with a nucleus of an atom within the sample. This causes the electrons to undergo an elastic collision. This produces other electrons to disperse, known as backscattered electrons. The second reaction occurs when the electrons from the focus beam collide with electrons within the sample. This collision is inelastic and as a result different forms of radiation are generated. This produces what is known as secondary electrons, which are picked up by a sensor. The sensor is known as the secondary electron detector and sends data to a computer. The computer then analysis the data and converts it into an image [53].

Image resolution is a function of the wavelength used. As visible light is of the order 380 nm, resolution is no better than this with a light microscope. Electrons used in an SEM operate at 20 keV have a wavelengths of 1 nm, hence far better resolution and magnification is possible. This finer wave length is able to fully "shine" on all parts of the surface [53].

### 2.    Testing Parameters

A Zeiss NEON 40 Field emission SEM with a focused ion beam was used for this study. High resolution images were taken using the "In Lens" setting at 20kV. The working distance for the images was 5 mm. Every sample was surveyed to examine the microstructure and two images were taken under different magnifications. These

magnifications were 50,000x, 100,000x, or 200,000x. Figure 26 is a picture of the SEM set up that was used for this study.
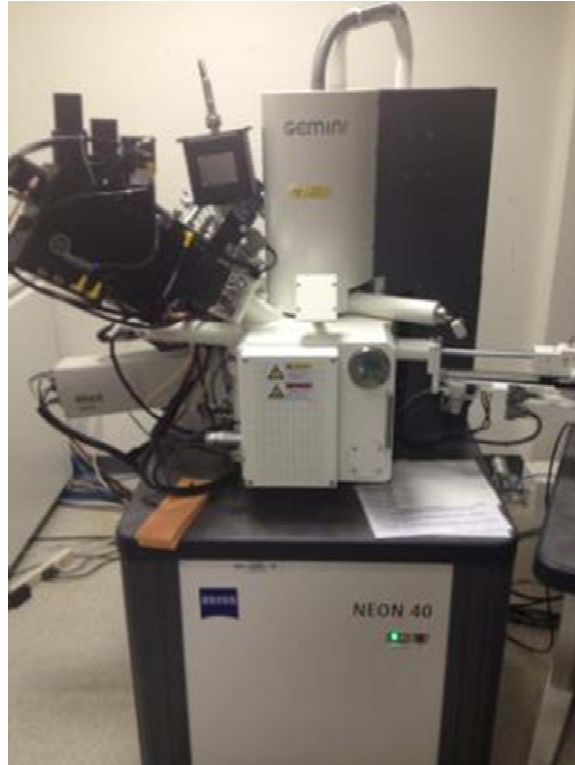


Figure 26.   This is a picture of the Zeiss Neon 40 Field emission SEM.

Prior to being examined in the SEM samples had to be prepared. This involved using double sided carbon tap to adhere a small amount of powder to the sample stud. This first involved sticking the double carbon tap to the sample stud holder and then pressing the sample stud into the powder. Using pressurized air loose material was removed. The loaded sample studs were then placed in container and placed in a vacuum chamber for 24 hours to remove any trapped moisture or air. Once "dried" the samples were removed from the vacuum and loaded onto a mounting platform. The SEM vacuum seal was then broken and the mounting platform was secured inside the SEM. Once secured the vacuum seal was reestablished for the SEM. The system settings were set to 20kV at $1.32\text{x}10^6$ mA, and strict compliance with NPS operating procedures were followed.

## C.    ENERGY-DISPERSIVE SPECTROMETER

### 1.    Purpose

The Energy-Dispersive Spectrometer (EDS) was used to examine unique particle structures that were observed in the SEM to determine their elemental composition. In addition a comparative analysis was conducted to compare the elemental composition of these structures to one another. The back bone on how the EDS is able to quantify the elements present in a sample is due to the x-rays that are given off by the sample [54].

The focused electron beam in the SEM penetrates the sample and interacts with the atoms that make up the sample. This results in the generation of two types of x-rays, Bremsstrahlung X-rays and Characteristic X-rays. Bremsstrahlung x-rays are generated when an electron from the primary beam comes in vicinity of the electric field of the surrounding nuclei of an atom. This causes the electron to slow down and deflect, thus loosing energy due to the inelastic scattering in the sample. Some of this loss in energy is converted into the form of X-rays, which have a lower energy state than the electron beam. Characteristic X-rays are generated when an electron from the primary beam ejects an electron from an atom's inner valance shell. This causes the atom to ionize and to become unstable. In order to maintain stability within the atom an electron from the outer shell fills the inner shell vacancy. As a result of this movement, an X-ray is released and has the energy equal to the difference between the ionized energies of the electrons involved in this process. Electrons in the K shell (the closest to the nuclei) produce the highest energy X-rays, while the conversely the outer shells produce lower energy X-rays [54].

It is the Characteristic X-rays that have a unique finger print that allows for elements to be identified. This is due to the fact that for each element the electrons in each shell and subshell have unique ionization energies. Since the Characteristic X-ray energy is due to the change of energy of filling electron it will produce a recognizable signature. Often more than one type of Characteristic X-ray with different energy will be released. The EDS uses a detector that records the X-ray intensity and the energy in eV. This will produce a pattern that allows the element to be identified. In addition, a

computer program can then be used to map out an entire area of a sample showing concentration of a particular element with in an area [54].

## 2.    Testing Parameters

For the purpose of this study an EDAX Pegasus system was used to conduct EDS analysis. Using SEM the sample was surveyed under 10,000 x magnification. Areas with unique particle structures were selected and scanned using the EDS to determine composition. Figure 27 is a picture of the EDS set up that was used for this study.



Figure 27.   This is a picture of the EDAX Pegasus system.

Prior to being examined by the EDS the samples had to be prepared in the same process as the SEM. Since double sided carbon tape was used to bond the sample to the sample holder it will limit the ability to accurately detect and analyze substances with carbon.    In addition, oxygen content is also difficult to be determined. Once the sample holder was secured to the sample mount the SEM vacuum seal was then broken and the mounting platform was then secured inside the SEM. Vacuum was then restored and the SEM was then used to survey the sample. After a particle of interest was found the EDS was used to identify its composition and an elemental x-ray map was conducted. The

scan settings were set to 60 μm at high current. Strict compliance with NPS operating procedures were followed at all times.

## D.  BET ANALYSIS

### 1.  Purpose

Stephen Brunauer, Paul Hugh Emmett, and Edward Teller developed an analysis technique that could be used to measure surface area of nano particles. A device was later developed and named using an acronym from the last names of the developers. It is desired to have a high surface area for a catalyst because it will be better suited for facilitating reactions. This device can measure surface area of these particles with great accuracy [55].

A BET analysis measures the surface area of nanoparticles by measuring the amount of gas that is adsorbed into the surface of the particles. In other words, it determines how much gas is sticking to the surface of the material. Using BET theory it is possible to estimate very accurately how many gas atoms, or molecules, are required to create an adsorbent layer on the surface of a particle. Using the number of atoms/molecules and multiplying it to area of the cross sectional area of the atom/molecule results in the surface area of the particle [56].

The process used in BET sounds very simple, although is a complex process and there are many factors that influence the adsorption of gas. For example the material properties of the gas, test sample, temperature, and pressure can drastically change properties of adsorption. Nitrogen is typically used as the adsorption gas because it has a strong interaction with most solid materials.   This interaction is still relatively weak; however, this can be overcome by using liquid nitrogen since it is able to adsorb more readily to the particles. When the sample is sufficiently cooled nitrogen gas fills the sample bulb. Nitrogen gas is then released in discrete increments, but the bulb continues to remain at partial vacuum. This is to insure that the ample achieves the saturation pressure, thus maximizing the adsorption rate. Pressure transducers are implemented to measure small changes in pressure due to the formation of adsorption layers. After the layers have formed, unabsorbed nitrogen gas is removed from the sample bulb. Finally

the sample is heated and all the gas that was adsorbed is released. The total amount of gas released is measured and plotted on an isotherm. A correction factor is used to increase the accuracy by using the samples weight before and after the process [57].

## 2. Testing Parameters

A NOVA 4200*e* Series Surface Area and Pore Size Analyzer (Figure 28) was implemented to conduct the analysis. It consists of two sections: degassing chamber and a BET analysis chamber. The degassing chamber is used to remove air, moisture, and other adsorbed gases. A vacuum pump removes gases from a test bulb, and heating mantles heat the bulb to further facilitate the process. The BET analysis chamber is where the actual measurements were taken and consists of flow lines that connect to a vacuum pump and nitrogen tank. In addition, there is a stage holder to hold a cylinder of liquid nitrogen that is used to cool the sample. An automatic controller regulates system pressure, and raises and lowers the sample bulb into the cylinder of liquid nitrogen. Test data was collect and stored on a computer.



Figure 28.   This is a picture of the NOVA 4200*e* Series Surface Area
and Pore Size Analyzer

BET measurements consist of a two stage process. The first stage is sample preparation and the second stage is the actual BET test. A sample is weighed and placed in a sample bulb. Care is taken to insure that particles are not settling along the sides of the glass leading to the bulb (failure to do so can throw off results). Once loaded the sample bulb is then placed inside the degassing chamber. The degassing process involves three steps. First the sample bulb is held at vacuum for 10 minutes. After 10 minutes the heating mantles are placed over the bulb and it is heated to $100^{o}$C for 30 minutes. Finally the sample is heated to $300^{o}$C for two and half hours. Once complete the sample bulb is then removed from the vacuum chamber and then loaded into the BET analysis chamber. Here the computer initiates an automated process that controls submerging the sample bulb into the liquid nitrogen cylinder, and when the nitrogen is supplied to the sample bulb. After the nitrogen is adsorbed onto the particles a vacuum is drawn on the bulb and it is removed from the nitrogen bath. The amount of nitrogen removed during this process is recorded as the sample bulb reaches vacuum and room temperature. When the testing is complete the sample is removed from the sample bulb and reweighed. This new weight measurement is entered into the computer so that a correction factor can be implemented and the results analyzed.

# IV.    RESULTS AND DISCUSSION

## A.    X-RAY DIFFRACTION

Before discussing the results of the XRD analysis data it is first important to discuss the amount of product generated and what precursors were used to produce it. Since the relative physical amount of phases in the product being analyzed will affect the number of counts, relative peak intensities will change. This should not affect the position of the peak intensity; however, elemental composition will change the peak locations. This can be used as an advantage to help quantify the present possible phases. Furthermore, because the precursors used, the only elements that should be present are nitrogen, hydrogen, oxygen, and molybdenum (with the addition of platinum for Experiment 11). Table 5 is a complete listing of the amount of product produced and the precursor mixture used to make it.

| Experiment | Precursor Mixture | Yield | Experiment | Precursor Mixture | Yield |
|---|---|---|---|---|---|
| 1 | 1.5 g $(NH_4)_6Mo_7O_{24}$ | 0.005 g | 7 | 0.75 g $(NH_4)_2MoO_4$ + 0.75 g Urea | 0.014 g |
| 2 | 1.5 g $(NH_4)_6Mo_7O_{24}$ | **0.000 g\*** | 8 | 0.75 g $(NH_4)_2MoO_4$ + 0.75 g Urea | 0.023 g |
| 3 | 1.5 g $(NH_4)_2MoO_4$ | 0.015 g | 9 | 0.75 g $(NH_4)_2MoO_4$ + 0.75 g Urea | 0.025 g |
| 4 | 1.5 g $(NH_4)_2MoO_4$ | 0.020 g | 10 | 0.75 g $(NH_4)_2MoO_4$ + 0.75 g Urea | 0.050 g |
| 5 | 1.5 g $(NH_4)_2MoO_4$ | 0.010 g | 11 | 0.75 g $(NH_4)_2MoO_4$ + 0.75 g Urea + 0.04 g $H_{12}N_6O_6Pt$ | 0.030 g |
| 6 | 0.75 g $(NH_4)_2MoO_4$ + 0.75 g Urea | 0.023 g | - | - | - |

Table 5.    This is a table listing of the total amount of product produce for each experimental run. Please note that there was no product collected during Experiment 2.

During Experiments 1 and 2 for this study was an attempt to molybdenum nitrides, however, such was not accomplished with the experimental conditions used in the plasma trials. Figure 29 is a plot of the XRD analysis on Experiment 1 that used only

$(NH_4)_6Mo_7O_{24}$ $4H_2O$ (dried) and argon gas. It is observed that there are several major intensity spikes at approximately 25.6, 27.3, 29.23, and 33.73 degrees ($2\theta$). Figure 30 displays the possible phases present. This sample possibly contains multiple phases of oxides: $Mo_9O_{26}$, $MoO_3$, and $Mo_4O_{11}$. No molybdenum carbides peaks were observed. Based off these observations the precursor was changed for Experiment 3.
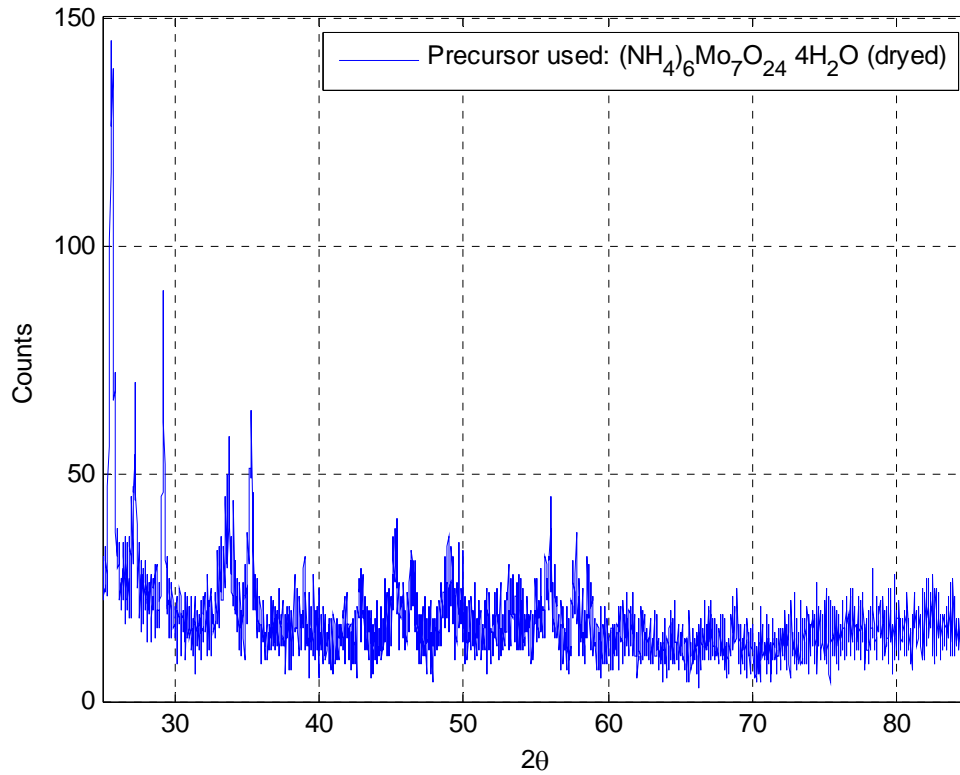


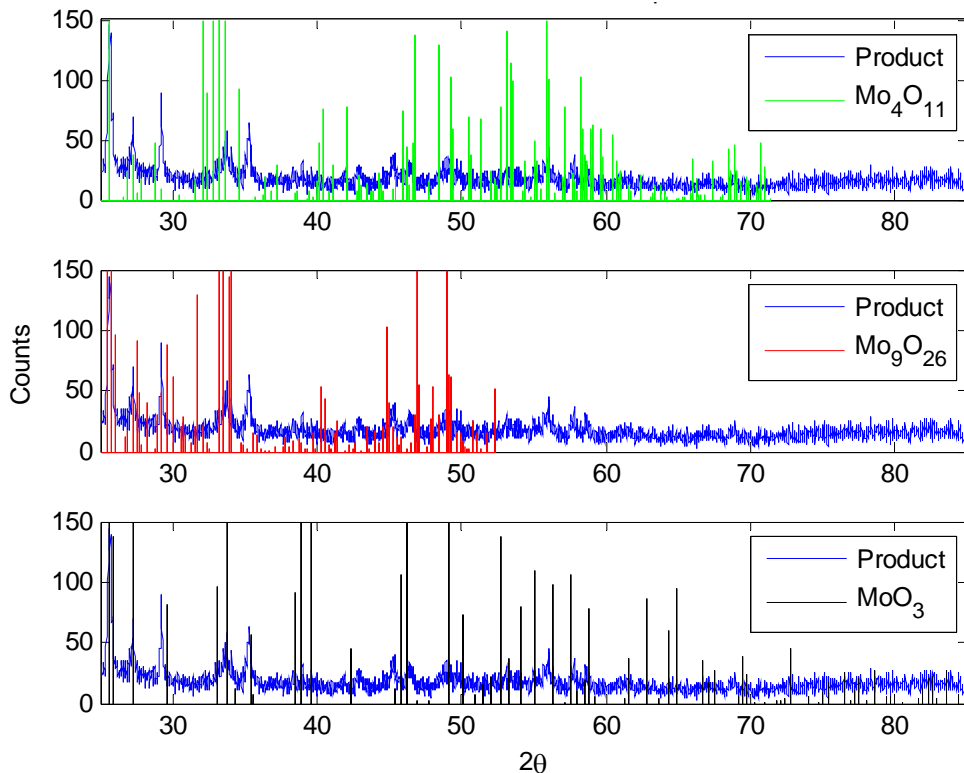Figure 29.   This is the results of the XRD analysis of Experiment 1.

Figure 30.   This plot shows the top three possible phases present within the product using the methods in Experiment 1.

In the experiment involving the use of nitrogen as the plasma and aerosol gas there was no product collected. This is due to the fact that the inner quartz tube used in the in the machine melted. The most likely cause of failure is probably due to the high temperatures seen in the plasma because nitrogen plasma ionizes hotter than argon. It was also observed during experimental runs that no product would jet through the quartz tube for a period of time before stopping. After disassembling the machine it was seen that precursor had coated the inner walls of the tube instead of flowing through. This suggests that the material was sticking to the surfaces of the tube and built up. As a result flow was restricted and allowing the temperature to rise to the melting point of the tube.

By analyzing the results presented above, it is evident that the amount of nitrogen groups provided simply by the precursor was not enough, even under nitrogen atmospheres, to produce the conditions in which a nitride will be stable as a solid phase. We decided to devote our efforts to the production of molybdenum carbide only. Figure

43

31 is a plot of the XRD analysis on Experiment 2 that used only $(NH_4)_2MoO_4$ and argon gas, used as a control group experiment. $(NH_4)_2MoO_4$ was chosen due to the fact that the molybdenum and oxygen ratios were lower than previous precursor thus making it more ideal to result in molybdenum carbide or nitride formations. Figure 32 shows that there is a strong match with $MoO_2$. No other significant phases were observed, but yielded a simpler XRD profile than Experiment 1. It is worth noting that the environment used to conduct the experiments avoided the introduction of oxygen groups from air (argon/nitrogen gas and overpressure conditions), being the precursor chemistry the only source of oxygen.
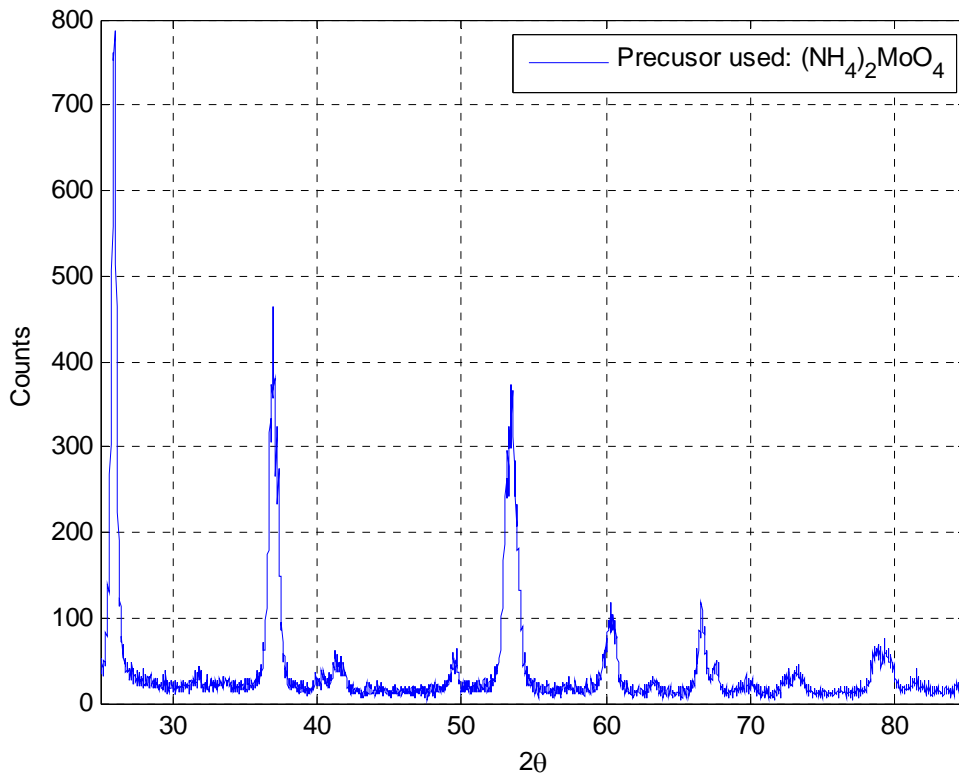


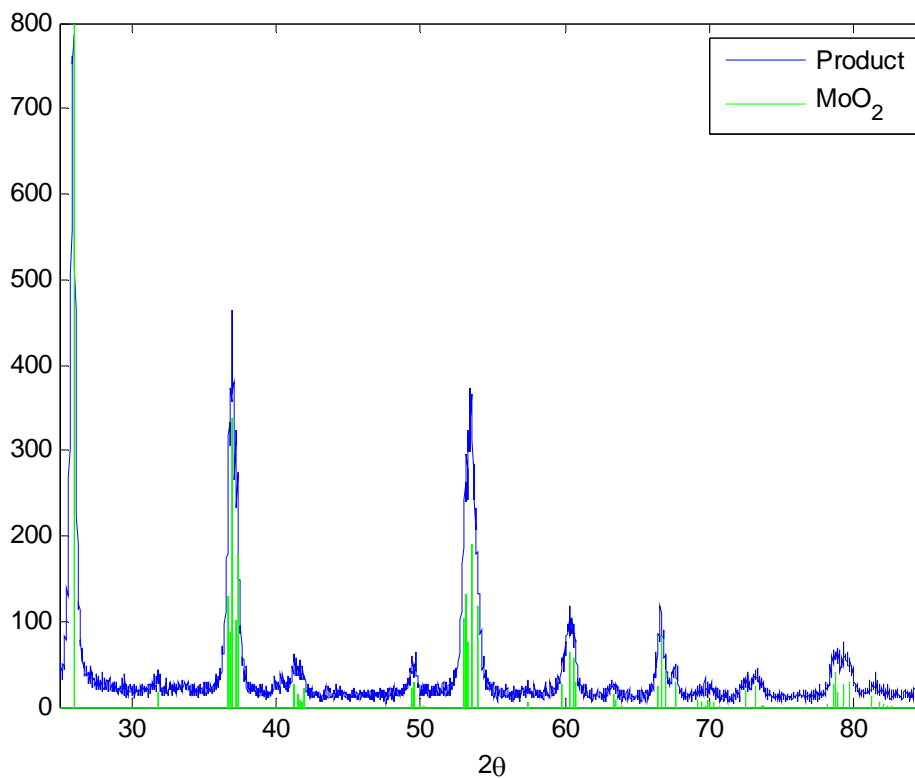Figure 31.   This is the results of the XRD analysis of Experiment 3.

Figure 32.   The plot shows the most probable phase present within the product from experiment 3.

In order to facilitate the formation of molybdenum carbides Experiments 4 and 5 used different aerosol gas mixtures, more prone to reduce the precursor oxygenated groups. Experiment 4 used argon with a 2% hydrogen gas and Experiment 5 used an ethylene/argon gas mixture. Figure 33 shows the results of this change. When compared to using only an argon aerosol (Experiment 3) the oxide peaks greatly reduced for both cases; however the ethylene/argon gas mixture was the most successful. This was because it was observed to have molybdenum carbides present (refer to Figure 34).
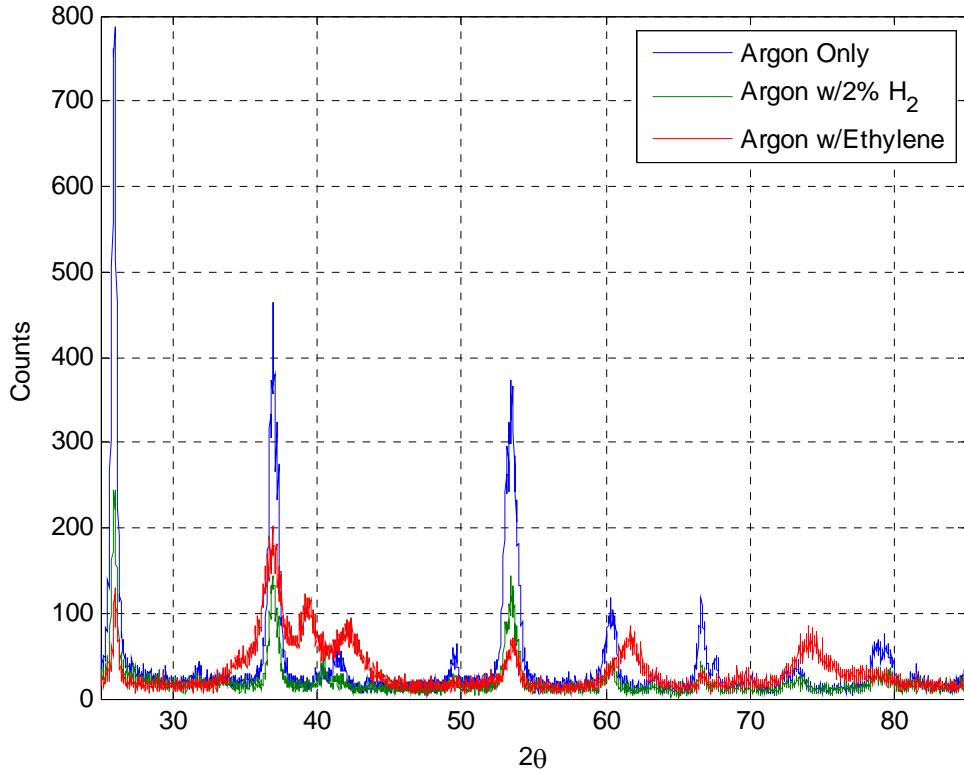
Figure 33.   This figure shows the results of using different aerosol gas mixtures in Experiments 4 and 5.

Figure 34. This plot shows the top five possible phases present within the product produced using the methods in Experiment 5.

For the next set of experiments the precursor was prepared as a mixture. This mixture consisted of 50 weight percent Urea and 50 weight percent $(NH_4)_2MoO_4$. Three experiments were conducted using this precursor mixture, but each one used a different aerosol gas mixture. Experiment 6 used only argon, Experiment 7 used argon with a 2%

hydrogen gas, and Experiment 5 used an ethylene/argon gas mixture. The results of this can be seen in Figure 35.
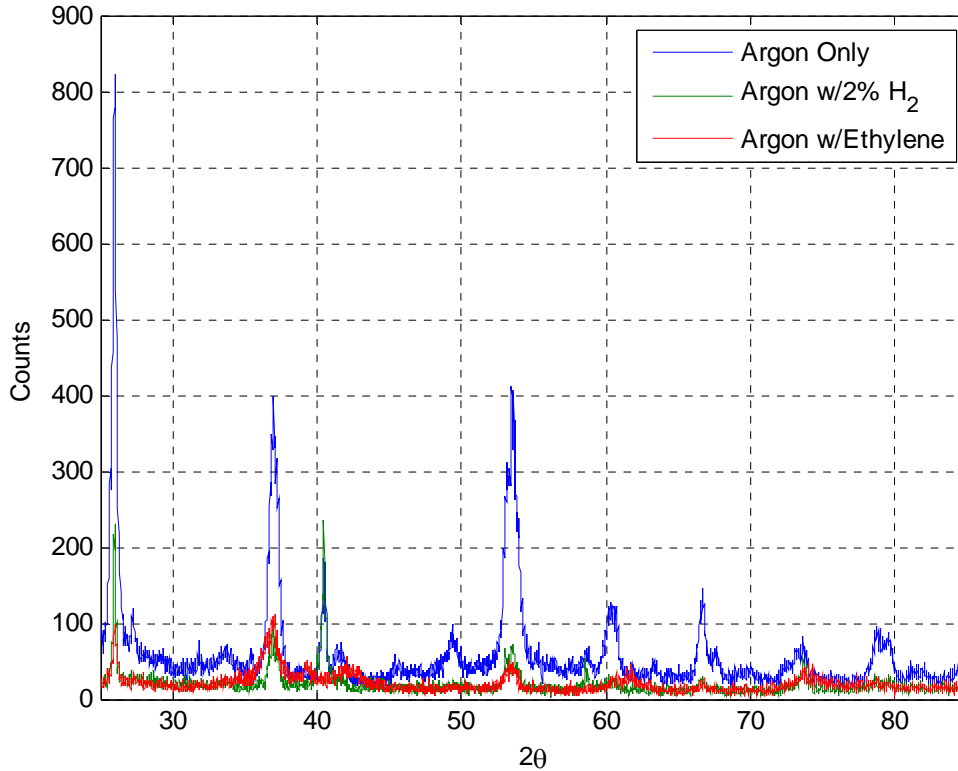


Figure 35. This figure shows the results of Experiments 6, 7, and 8 by using the mixed precursor processed under different aerosol gas mixtures.

Experiment 8 produced desirable results as once again the argon/ethylene gas mixture proved to be superior over the argon with 2% hydrogen used in Experiment 7 because it produced larger amounts of the phases of interest. Interestingly Experiment 7 still provided an interesting discovery to the ATP process. Experiment 7 showed phases that indicate pure molybdenum. This is important for the fact that in certain materials manufacturing processes it is desirable to have small pure material powders. These powders can be mixed together and pressed/injected into a mold to produce a part. How small the part can be is restricted by the size of the powders used. Currently predominate method of producing small pure powders is through atomization that results in a particle size of 1 μm. The ATP process has reported particle sizes in the nano scale [42]. This

could allow for the manufacture of smaller high quality parts. Figures 36 and 37 show the possible phases present within the products using the methods in Experiments 7 and 8.
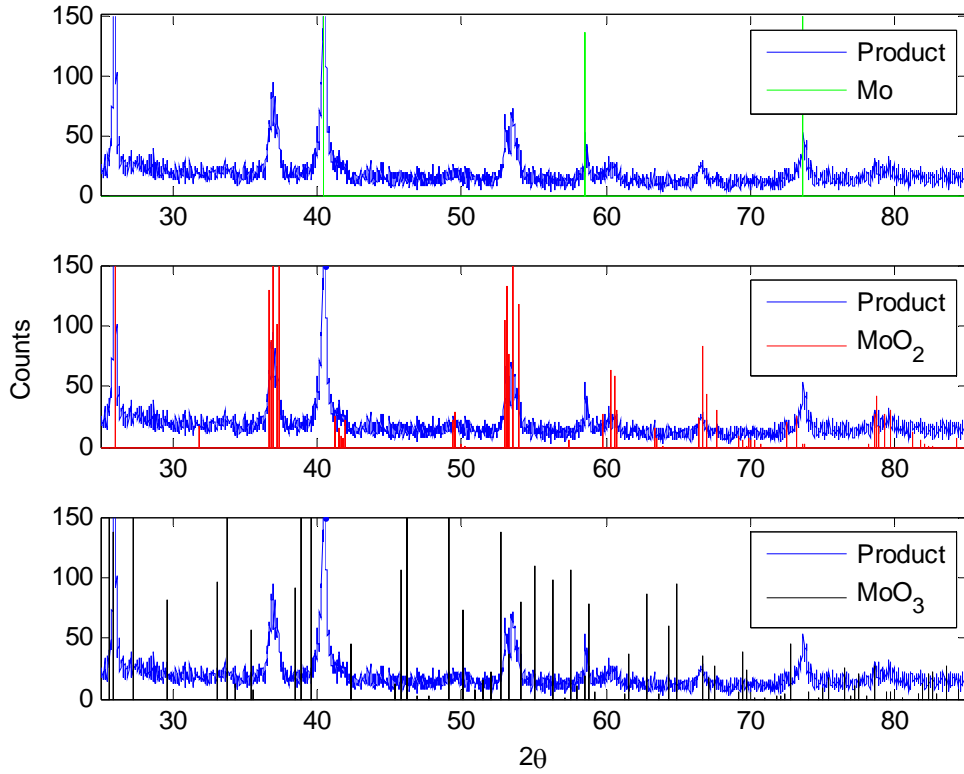


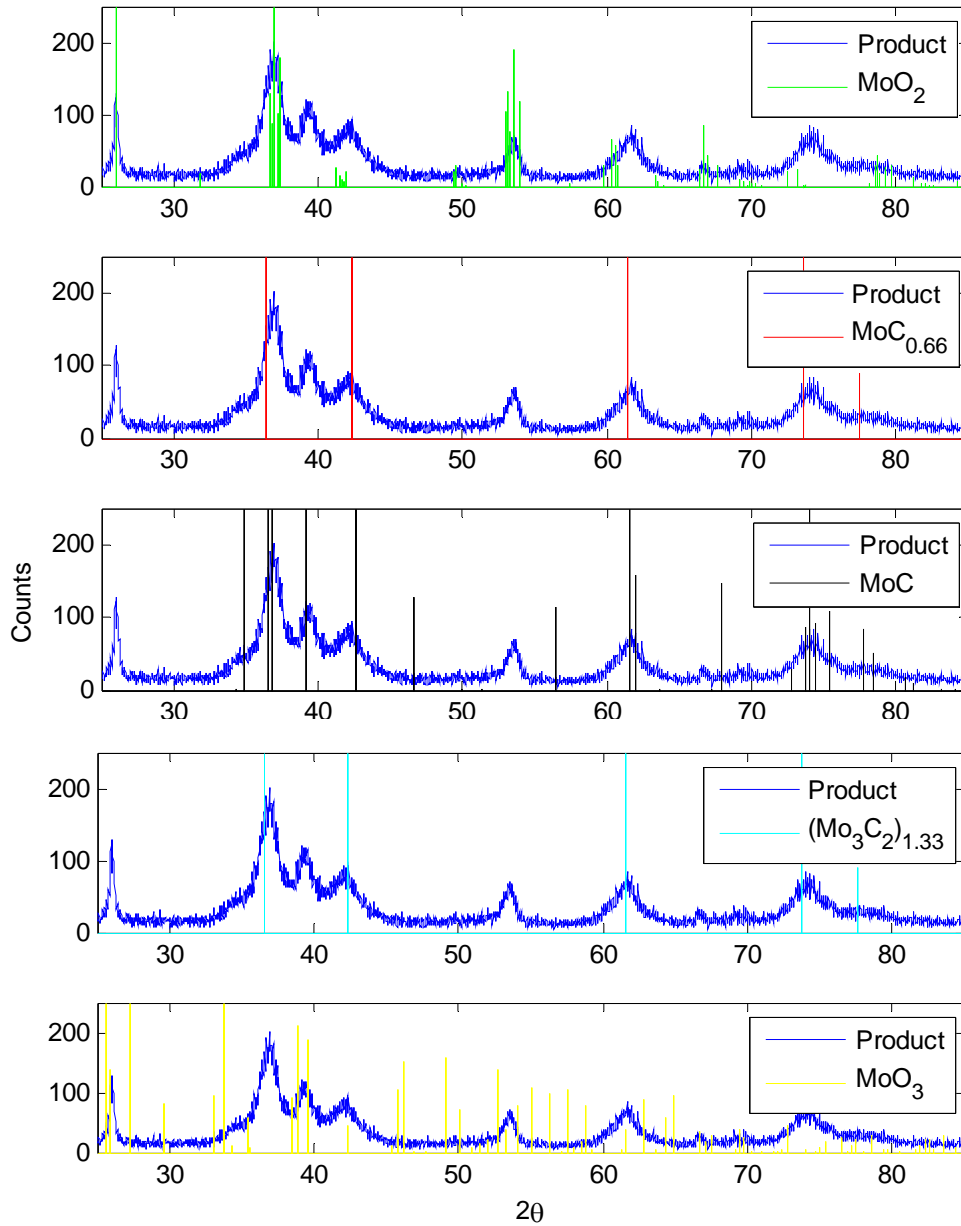Figure 36.   This plot shows the top three possible phases present within the product using method in Experiment 7.
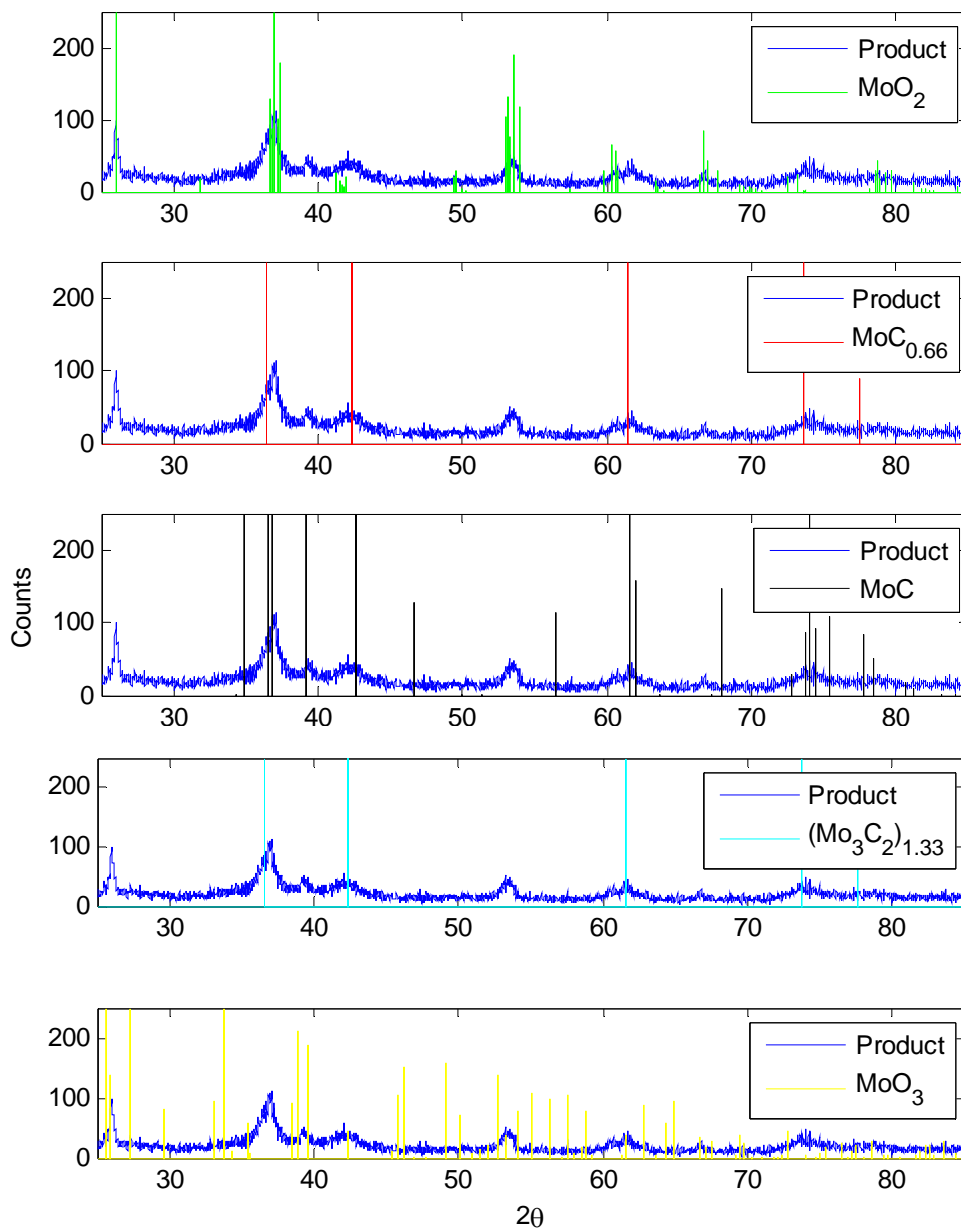
Figure 37. This plot shows the top five possible phases present within the product using method in Experiment 8.

For Experiments 9 and 10 it was intended to determine how the amount of ethylene would change the molybdenum oxide and carbide peak intensities. For Experiment 9 the ethylene flow rate was increased from 0.075 g/min to 0.100 g/min and Experiment 10 increased to 0.128 g/min. Figure 38 shows the results of increasing the flow rate of ethylene. The oxide peaks decreased while the carbide peaks increased as the

flow rate of ethylene was increased. This suggest that it is possible to increase the ethylene such that all the oxygen is scavenged; however due to safety considerations it is capped at 0.128 g/min. Figure 39 shows the possible phases present in the product produced using the method in Experiment 10. It can be seen that there are many different forms of molybdenum carbides present (MoC, $Mo_2C$) and a molybdenum oxide phase ($MoO_2$). In addition, there is the possibility that molybdenum nitride could be present, but there is no way to be sure because the peaks are convoluted with the carbide and oxide peaks.



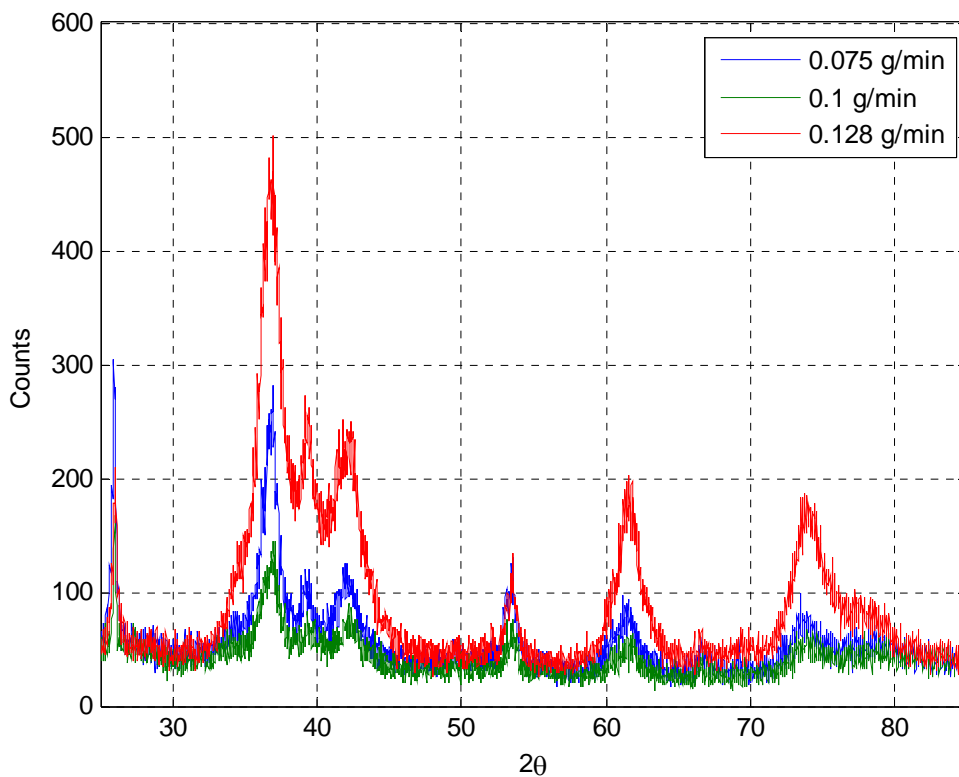Figure 38.   This figure shows the results of Experiments 8, 9, and 10 by increasing the flow rate of ethylene.
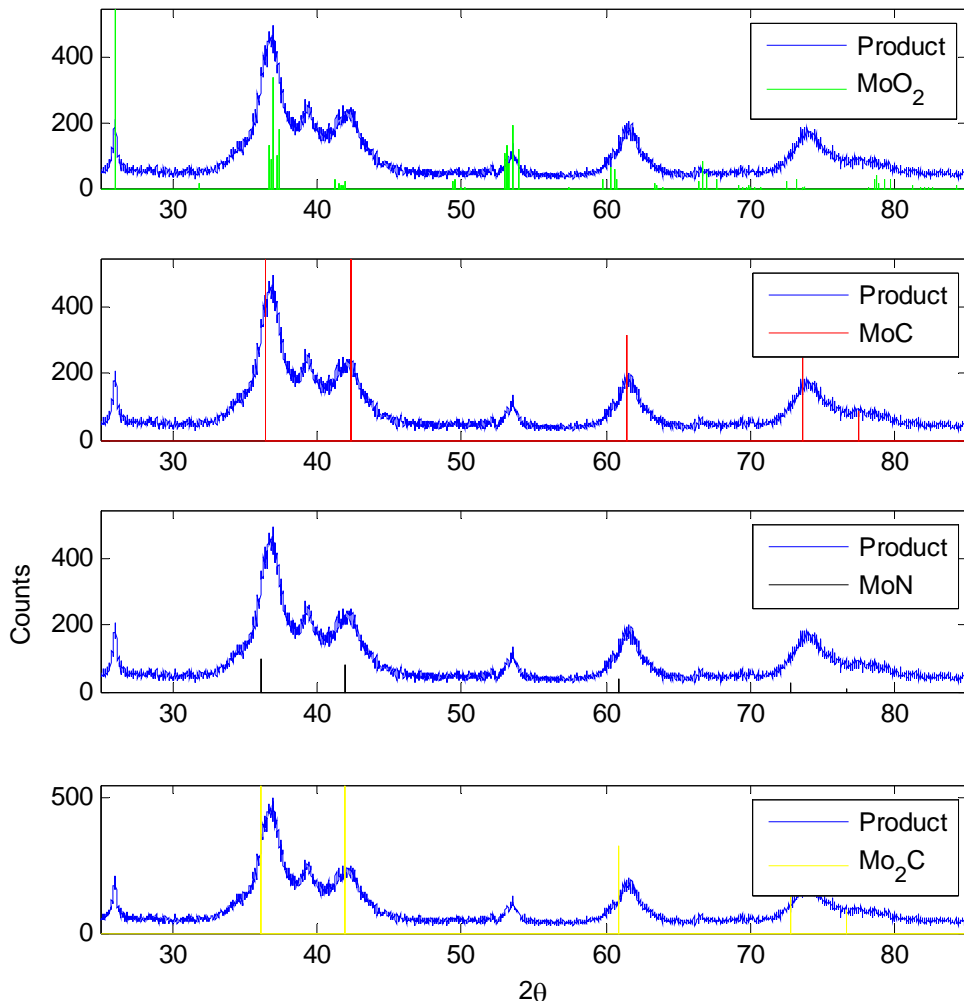
Figure 39.   This plot shows the top five possible phases present within the product.

Finally, Experiment 11 was designed to produce a useable catalyst by employing the best parameters for creating Mo2C but making the adjustment of adding a relatively small quantity of a platinum containing molecule. This was accomplished by adding tetramine platinum nitrate to the 50/50 urea and $(NH_4)_2MoO_4$ precursor mix so that there was 5 weight percent platinum. The precursor was processed using the method developed in Experiment 10. Figure 40 shows the possible phases present in the catalyst. The catalyst has a very similar profile to Experiment 10 with many forms of molybdenum carbides (MoC, $Mo_2C$) and molybdenum oxide ($MoO_2$) phases present. There was a platinum phase profile added to the figure as a reference to show that there were no noticeable matching peaks. Prior work suggests this means the platinum can be

remarkably well dispersed on $Mo_2C$, perhaps present only as 'rafts' containing less than 10 atoms. Indeed, using a chemical process, called 'Nano-Raft' very highly dispersed Platinum structures have been produced. Experiments indicate these materials are extremely durable, far more durable than the best commercial fuel cell catalysts. This is quantified in Figure 7. Clearly the commercial catalyst, 'C/Pt' loses virtually all activity over 5000 accelerated aging cycles, whereas catalyst Mo2C/Pt (3) loses virtually no activity over the same test period. An XRD study of the latter reveals no Pt structures. Detailed TEM studies showed that the Pt in Mo2C/Pt (3) was present as 'rafts' with no more than 6 atoms/raft. Not surprisingly, structures of this scale do not diffract sufficiently to be observed using standard XRD equipment [34].
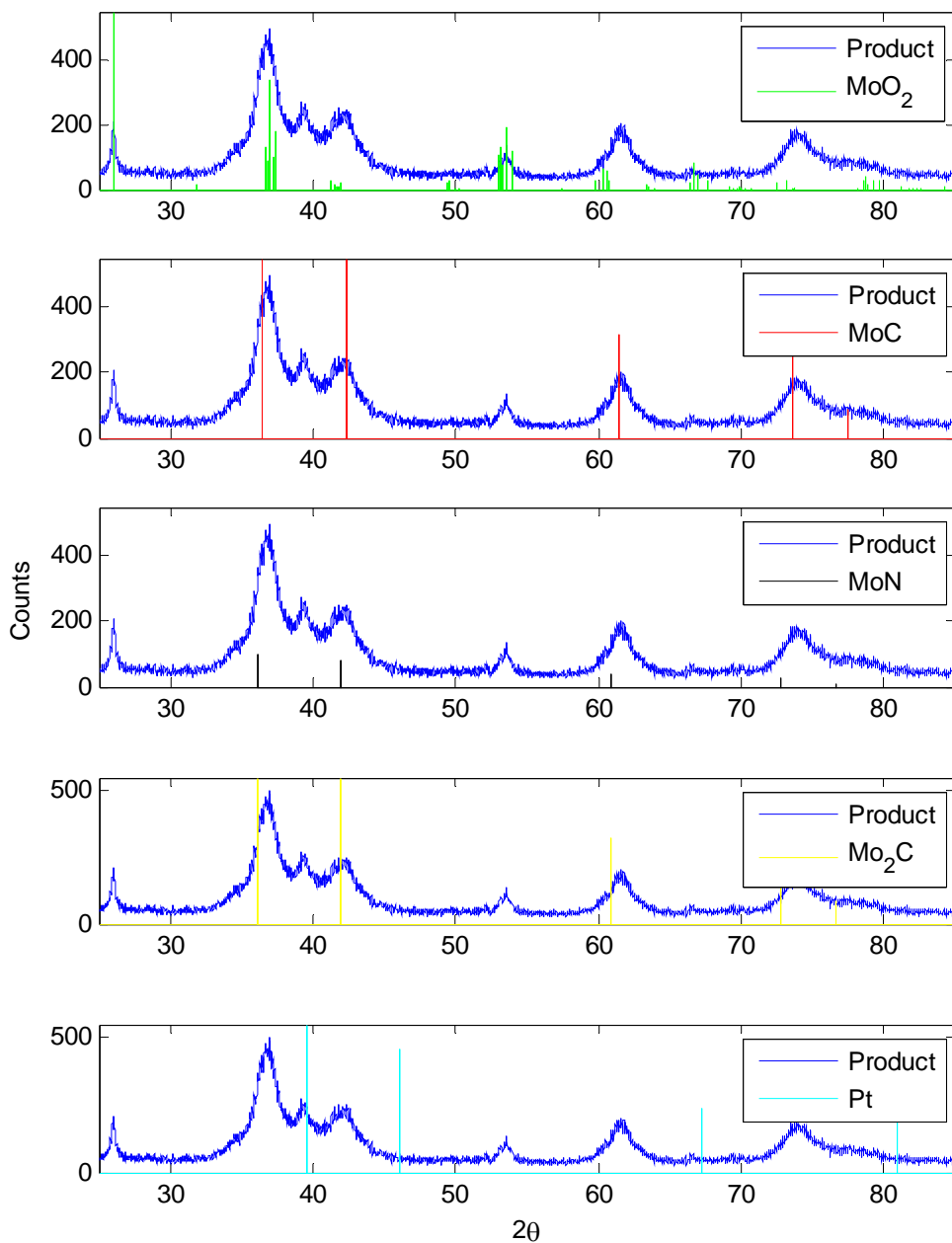
Figure 40. The top plot shows the XRD profile of Experiment 11 with overlays of possible matches. The bottom plot is a break out of the possible matches.

## B. SCANNING ELECTRON MICROSCOPE RESULTS

The SEM was used to examine the microstructure of the catalyst produced in Experiment 11. It was observed that there were many types of crystalline structures

present within the material, but only three were observed with high frequency. These structures vary in size, shape, and are observed throughout the catalyst. This was expected due to the nature of the ATP process and phases examined in the XRD analysis [42].

Figures 41 and 42 were taken at 50,000x and 200,000x magnification. They show two types of structures present. The first structure appears to be block like and is often clustered near other blocks. This structure is often smooth, but sometimes will have concave indentations. It was observed that the particle structure size ranged from 300 nm to 700 nm. When these structures were seen they were always accompanied by small specks. Upon further magnification these specks were spherical or elliptical in nature. The average size of these spherical structures was 30 nm in diameter.
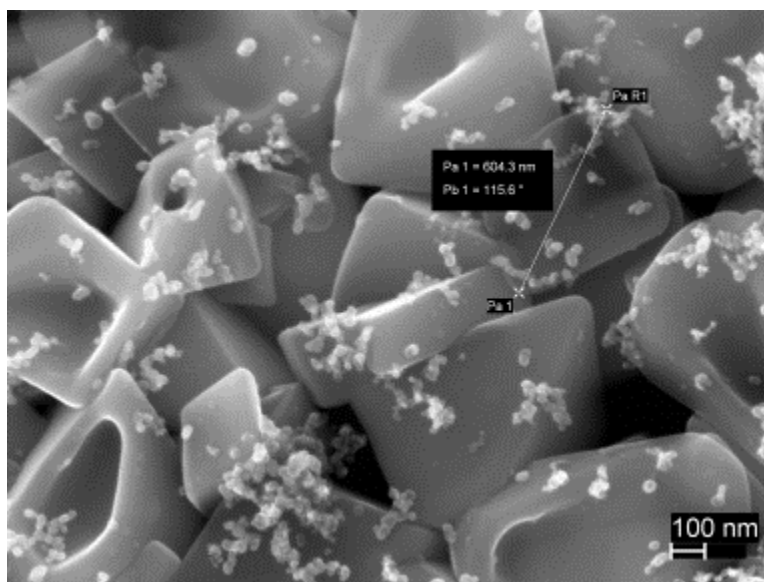


Figure 41.   SEM image at 50,000x magnification depicting a block like structure.
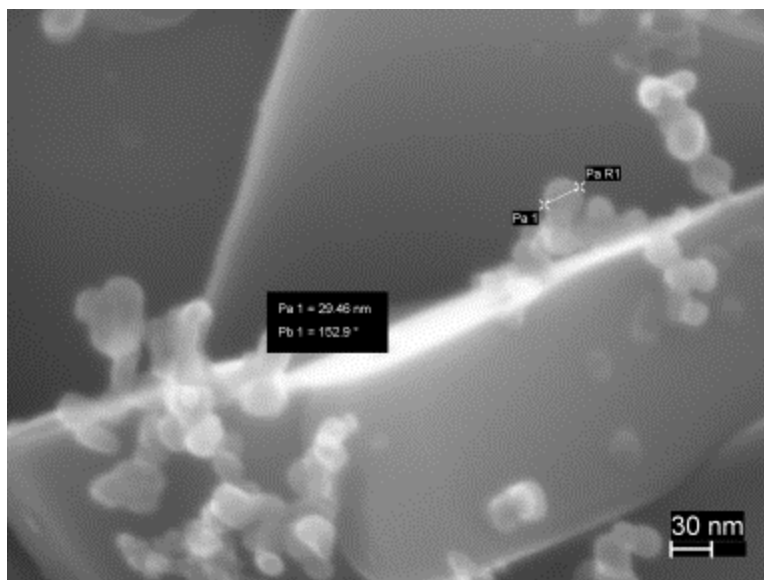
Figure 42. SEM image at 200,000x magnification focusing on the presence of small
sphere like structures that appear near the block structures.

The next structures observed can be seen in Figures 43 and 44. Both figures were taken at 50,000x magnification and it can be seen that there are needle like structures present. These needles are approximately 44 nm in diameter and range in 200 to 350 nm in length. In the upper left hand corner of Figure 44 it can be seen that there is another microstructure present with the needles. This structure is rare and is found throughout the catalyst with other structures. It measures from 250 to 350 nm across and tends to form a rough block like structure.
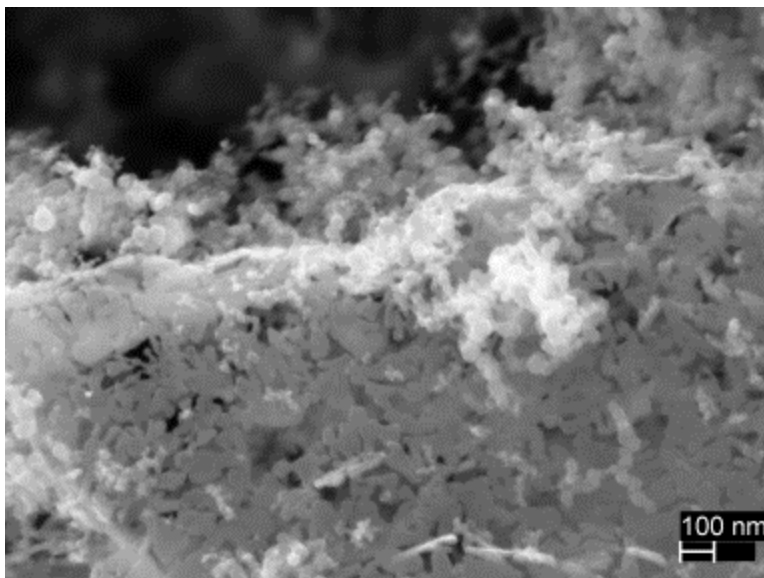
Figure 43.  SEM image at 50,000x magnification examining needle like structures.
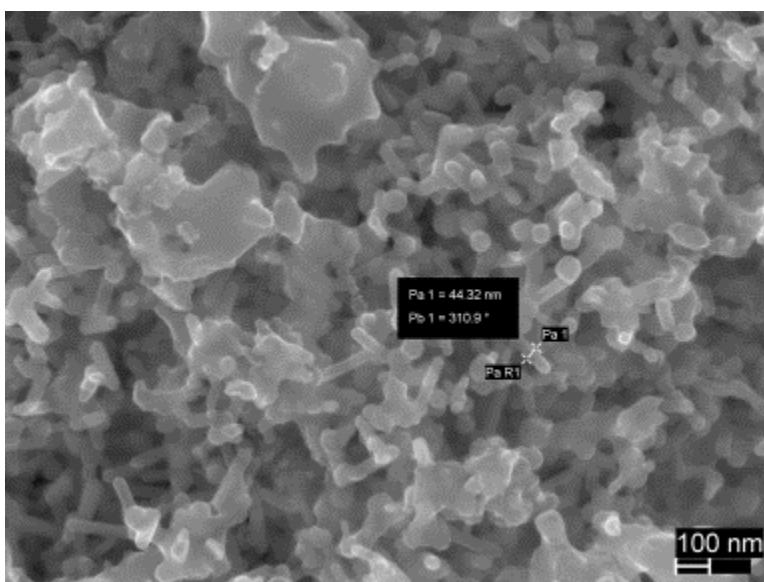


Figure 44.  SEM image at 50,000x magnification that shows the diameter of the needle like structures. The rough block like structures can be observed in the upper right hand corner of the image.

Finally Figures 45 and 46 show the last type of structure found in the catalyst. This structure tends to have agglomerate like shape. It is the most common structure found within the catalyst and ranges from 25 nm to 50 nm in size. These structures could be similar to the ones found in Figure 42 but are bigger and more oddly shaped.

57
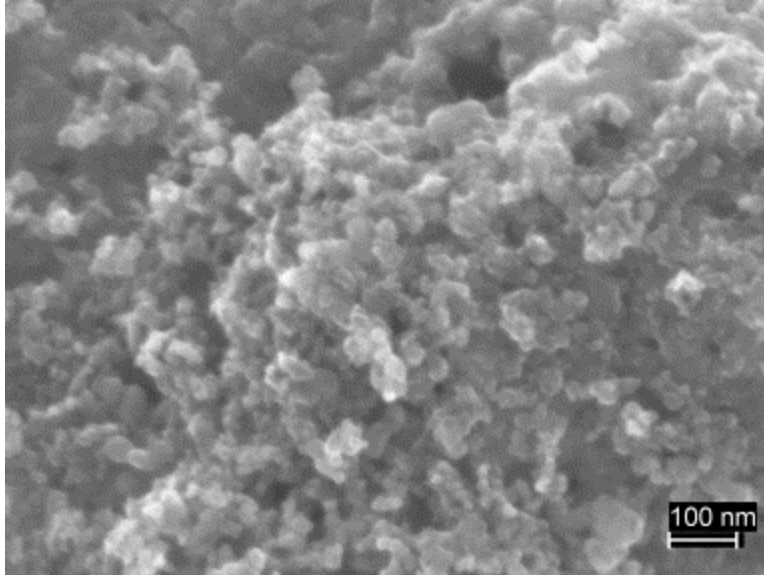
Figure 45.   SEM image at 100,000x magnification that shows agglomerate like structure.
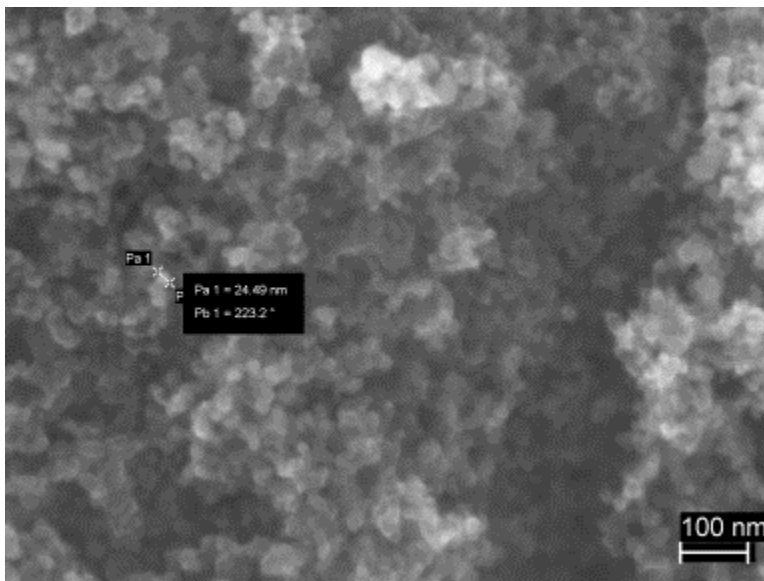


Figure 46.   SEM image at 100,000x magnification that depicts the average size of the "agglomerate" like structure.

## C.   ENERGY-DISPERSIVE SPECTROMETER

EDS was used to examine the three most predominately found structures during the SEM analysis: the blocks, needles, and agglomerate like structures. The result of using the EDS on these structure sites does not fully characterize the structures elemental

composition. This is due to the fact the particle size is very small and the electron beam used to point identify the structures isn't small enough. This results in other structures producing x-rays that are detected and displays elements that are not actually present. Another factor is that, since carbon tape was used in the sample holder to glue the sample to the holder, it could drastically alter any carbon findings. With this said, the EDS results were mainly used to compare the elemental composition of each of the structures to one another.

The first structure to be analyzed by the EDS was the blocks. Figure 47 is a two part figure. The left side shows the elements present and the right side shows the area that it was taken. The element readily detected was molybdenum with traces of oxide, but interestingly there were also trace amounts of platinum detected. A semi-quantitative analysis was conducted for molybdenum and platinum (oxygen and carbon were excluded). It was observed 98 weight percent was molybdenum and only 1.95 weight percent was platinum. Based off this result, it is plausible that there are platinum sites, but due to the small amount the blocks are most likely a molybdenum structure. This could be explained in the base that pure molybdenum in atmosphere will oxidize over time. The oxygen content when compared to other EDS scan sites is relatively higher than other locations. Unfortunately, due to their small size, the spherical particles that were observed near the block structures in the SEM could not be analyzed.
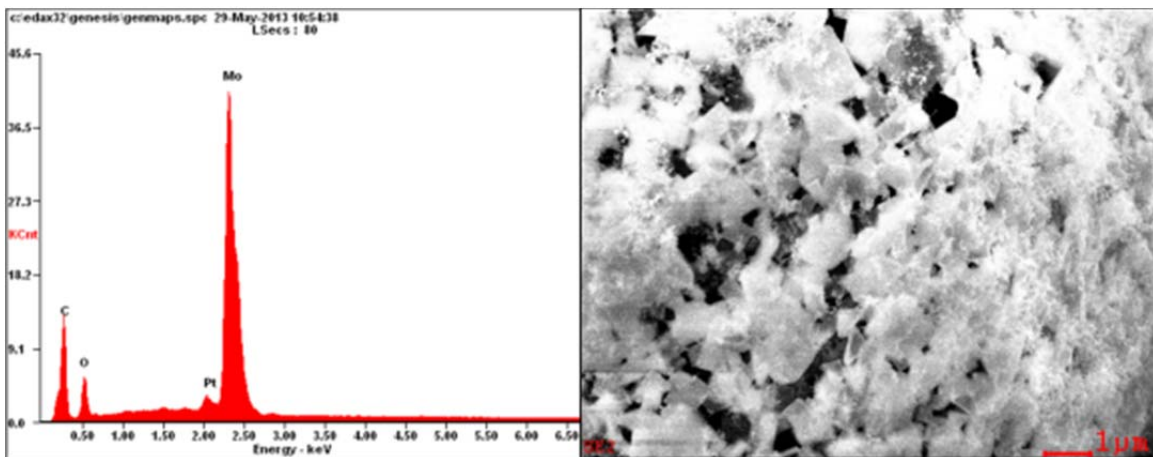


Figure 47.   10,000x magnification EDS scan of the block like structures.

The next structure to be analyzed was the needle structures. Figure 48 shows the two different areas that were analyzed using the EDS. The left side shows the results of the scans and the right side contain images of the scanned area framed by a red box. It was observed that molybdenum was predominately present with some oxygen. This could suggest that the sites are in habited by molybdenum oxides. Interestingly, silicon was detected and most likely came from the quartz tube that is used in the plasma torch.
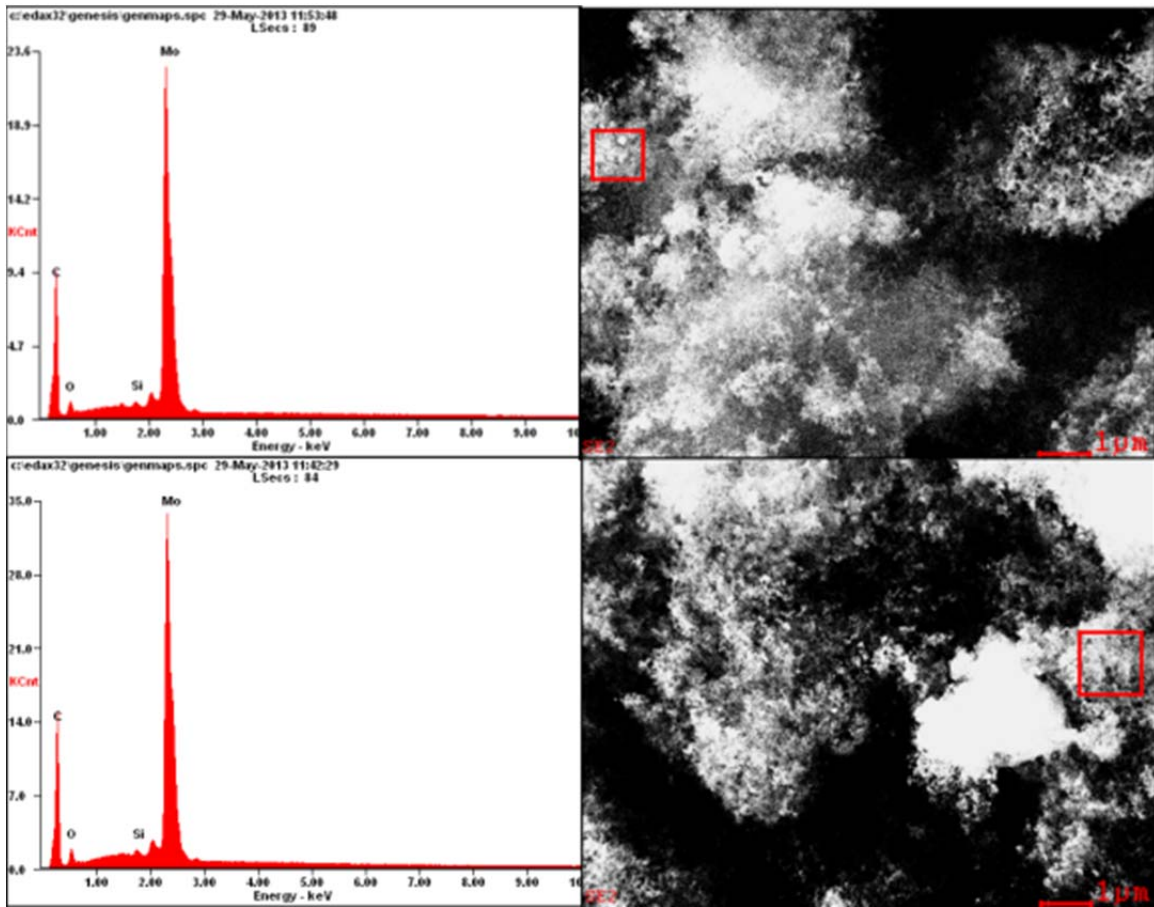


Figure 48.   10,000x magnification EDS scan of needle structure sites.

The final structure analyzed by the EDS was the "agglomerate" like structure. Figures 49 show the results of EDS analysis of these sites. Even though the presence of oxygen was detected these scans yield the most interesting results. The carbon peak intensity is four to five times greater here than anywhere else in the sample. It should be noted that these scans were conducted far away areas where the carbon tape was exposed,

and that the catalyst was the thickest. This could possibly suggest that there are carbide or amorphous formations present in these areas.
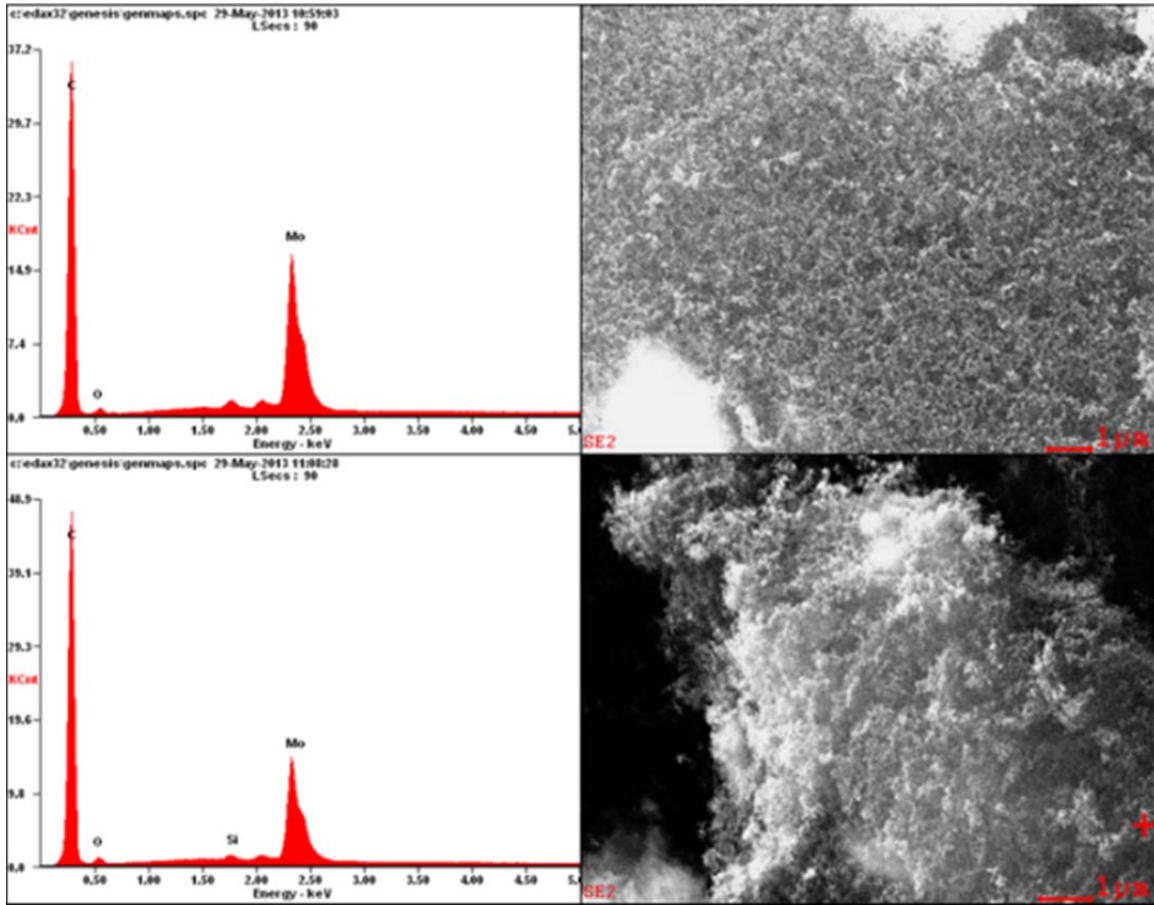


Figure 49.   10,000x magnification EDS scan of "agglomerate" structure sites.

## D.      SURFACE AREA TESTING

The BET analysis on 0.020 grams of the final support catalyst yielded unexpected results. It was observed that when it was collected off the filter or the chimney of the plasma torch that it exhibited a high volume for its mass. For the BET testing it was required to degas the sample beforehand. This involved at one point heating the sample in a vacuumed environment up to $300^{\circ}C$ for two and half hours. After degassing the sample was tested in the BET. The test yielded a result of 1 $g/m^2$ surface area. When the sample was taken out of the test cell it was observed to have reduced volume and had a mass of 0.010 grams. It is likely that the degassing procedure used agglomerated the sample

thereby locking in some of the surface area and making it not accessible for nitrogen adsorption. In any case, the treatment modified the nature of the powder sample.

# V.    SUMMARY AND CONCLUSIONS

This study provided insight into making molybdenum nitride and carbide catalysts using the ATP method. Even though there is no sufficient data to suggest that molybdenum nitrides were created it is possible to produce small molybdenum carbides using plasmas; however, more refinement is still required to yield high surface area molybdenum carbides with no oxide phases present. When it is fully refined this process can produce molybdenum carbide catalysts in a very simple manner. It should be noted that a large amount of catalyst was created using this method and sent off to Los Alamos for fuel cell testing. As of June 1, 2013 LANL collaborators had incorporated the ATP material in an MEA and fuel cell testing studies initiated. A report on results is expected shortly.

It was proven that by changing the precursor mixture or using a different gas mixture can significantly alter the final catalyst product. By observing the results of each production in the XRD adjustments could be made to the baseline precursor or aerosol gas mixture. Adjustments to the ethylene flow rate showed a reduction in oxide phases, and increase in carbide phases. In addition it was observed in the SEM that particle sizes ranged from 30 nm to 350 nm. Unfortunately, the relative surface area was questionable due to the procedures used in the degassing; however, if the surface area really 1 $g/m^2$ it will have a profound impact in performance characteristics of the support catalyst.

It is highly recommended that a follow on study take place to improve and build upon the results of this study.   The first of which is to develop a better ATP set up. It is possible that oxygen is getting into the system causing undesirable reactions, such as oxide formation. It likely a better sealing mechanism is needed where the precursor is transformed into an aerosol. In addition, production runs using the ATP method produced very little amount of product, thus making it difficult to characterize and test each sample. A better means to deliver a steady stream of aerosol to the plasma is desired in order to improve the yield.

Another route to take this study is experimenting with other precursors or changing the aerosol gas mixtures. In this study it was observed by switching the base line precursor would yield drastically different results. This is due to the fact that different elemental compositions within a precursor mix will break down in a different manner. As a result they will recombine in a different manner that would allow carbide formations, or produce a molybdenum powder. Likewise, using different aerosol gas mixtures (e.g., a propane/argon) will probably prove to be a better oxygen scavenging agent. With these suggestions it is possible that a more desirable molybdenum ceramic support catalyst could be developed or a small sized molybdenum powder using the ATP process.

# LIST OF REFERENCES

[1]     "National Security Strategy May 2010," Available from the World Wide Web: http://www.whitehouse.gov/sites/default/files/rss_viewer/national_security_strategy.pdf, Last retrieved on 16 May 2013.

[2]     President Barack Obama, "State of the Union," Available from the World Wide Web:  http://www.whitehouse.gov/state-of-the-union-2013, Last retrieved on 16 May 2013.

[3]     U.S. DOE, "The Department of Energy Hydrogen and Fuel Cell Plan," Available from the World Wide Web: http://www.hydrogen.energy.gov/pdfs/program_plan2011.pdf, Last retrieved on 16 May 2013.

[4]     A. J. Appleby and F. R. Foulkes, "*Fuel Cell Hand Book*," New York: Van Nostrand Reinhold, 1989.

[5]     J. Bellingham, L. Brewer, J. Farmer, S. Oswald, and K. Wolf,  "ME4901 Course Notes Special Topics in Energy Conversion & Storage," United States Naval Postgraduate School, Mechanical & Aerospace Engineering Department, LLNL-MI-464396

[6]     V. Mehta and J. S. Cooper, "Review and analysis of PEM fuel cells design and manufacturing," *Journal of Power Sources*, vol. 114, pp. 32–53, 2003.

[7]     S. Gottesfeld and T. Zawodzinski, "Polymer electrolyte fuel cells," *Advance Electrochemical Science & Engineering*, vol. 5, pp. 15–301, 1997.

[8]     X. Glipa and  M. Hogarth, Department of Trade and Industry (UK) Homepage, 2001. Available from World Wide Web: http://www.dti.-gov.uk/renewable/pdf/f0200189.pdf. , Last retrieved on 1 Dec 2011.

[9]     J. J. Conley, T. J. Fuller, H. A. Gasteiger, C. J. Gittleman, S. S. Kocha, R. Makharia, M. F. Mathias, D. P. Miller, C. K. Mittelsteadt, T. Xie, and S. G. Yan, P. T. Yu, "Two Fuel Cell Cars in Every Garage?" The *Electrochemical Society Interface*, Fall 2005

[10]    DuPont Home page, Nafion Membranes, "Safe Handling and Use," Available from the World Wide Web: http://www2.dupont.com/FuelCells/en_U.S./assets/downloads/dfc301.pdf, Last Retrieved on 16 May 2013.

[11]    M. Rikukawa and K. Sanui, "Proton conducting polymer electrolyte membranes based on hydrocarbon polymers," *Progress in Polymer Science*, vol. 25 pp. 1463–1502, 2000.

[12]    A. L. Dicks, "Hydrogen generation from natural gas for the fuel cell systems of tomorrow," *Journal of Power Sources*, vol. 61, pp. 113–124, 1996.

[13]    M. Boe, J. Bogild-Hansen, P. Brockerhoff, G. Colsman, B. Emonts, B. Hohlein, R. Menzer, and E. Riedel, "Hydrogen from methanol for fuel cells in mobile systems: development of compact reformer," *Journal Power Sources*, vol. 61, pp. 143–147, 1996.

[14]    R. Parsons and T. VanderNoot, "Utilization of methanol for polymer electrolyte fuel cells in mobile systems," *Journal of Power Sources,* vol. 49, pp. 299–313 1994.

[15]    W. Lee, R. Mohtadi, and J. W. Van Zee, "Assessing durability of cathodes exposed to common air impurities," *Journal of Power Sources*, vol 138, pp. 216–225 ,2004.

[16]    S. Y. Ahn, Y. C. Lee, T. W. Lim, H. Y. Ha, S. A. Hong, I. H. Oh, and S. J. Shin, "Performance and life time analysis of the kW-class PEMFC stack," *Journal of Power Sources*, vol. 106, pp. 295–303, 2002.

[17]    A. Collier, H. Wang, D. P. Wilkinson, X. Z. Yuan, and J. Zhang, "Degradation of polymer electrolyte membranes," *International Journal of Hydrogen Energy*, vol 31, pp.1838–1854, 2006.

[18]    M. Watanabe and S. Motoo, "Chemisorbed CO on a polycrystalline platinum electrode the effect of conditioning of the surface and of partial pressure of CO," *Journal of Electroanalytical Chemistry and Interfacial Electrochemistry*, vol, pp. 197–208, 1986.

[19]    T. Fujino, H. Igarashi, and M. Watanabe, "Hydrogen electro-oxidation on platinum catalysts in the presence of trace carbon monoxide," *Journal of Electroanalytical Chemistry*, vol 391, pp. 119–123, 1995.

[20]    J. C. Amphlett, R. F. Mann, B. A. Peppley, P. R. Roberge, and A. Rodrigues, "Carbon monoxide poisoning of proton-exchange membrane fuel cells," *Proceedings of the thirty second intersociety Energy Conversion Engineering Conference*, pp. 768–773, 1997.

[21]    H. F. Oetjen, V. M. Schmidt, U. Stimming, and F. Trila, "Performance Data of a Proton Exchange Membrane Fuel Cell Using H2/CO as Fuel Gas," *Electrochemical Society*, vol. 143, pp. 3838–3842, 1996

[22]  J. Divisek, H. F. Oetjen, V. Peinecke, V. M. Schmidet, and U. Stimming, "Components for PEM fuel cell systems using hydrogen and CO containing fuels," *Electrochimica Acta*, Vol. 43, pp. 3811–3815, 1998.

[23]  P. A. Adcock, S. V. Pacheco, K. M. Norman, and F. A. Uribe, "Transition Metal Oxides as Reconfigured Fuel Cell Anode Catalysts for Improved CO Tolerance: Polarization Data," *Journal of Electrochemistry Society*, vol 152, pp. A459–A466, 2005.

[24]  F. Lufrano, E. Passalacqua, A. Patti, and G. Squadrito "Advanced CO Tolerant Anodes for Polymer Electrolyte Fuel Cells (PEFCs)," *Hydrogen Power: theoretical and Engineering Solutions*, pp. 591–596, 1998.

[25]  M. Gotz and H. Wendt, "Binary and ternary anode catalyst formulations including the elements W, Sn and Mo for PEMFCs operated on methanol or reformate gas," *Electrochimica Acta*, vol. 43, pp. 3637–3644, 1998.

[26]  S. L. Clauson, G. L. Holleck, and D. M. Pasquariello, "Carbon monoxide tolerant anodes for proton exchange membrane (PEM) fuel cells. II. Alloy catalyst development," *Electrochmical Socity Proceedings*, vol. 98–27, pp. 150–160, 1999.

[27]  F. A. de Bruijn, M. Keijzer, D. C. Papageorgopoulos, and J. B. Veldhuis, "CO Tolerance of Pd-Rich Platinum Palladium Carbon-Supported Electrocatalysts Proton Exchange Membrane Fuel Cell Applications," *Journal of Electrochemical Society*, vol. 149, pp. A1400–A1404, 2002.

[28]  G. Garcia, O. Guillen-Villafuerte, E. R. Gonzalez, E. Pastor, J. L. Rodriguez, and J. A. Silva-Chong, "CO tolerant catalysts for PEM fuel cells: Spectroelectrochemical studies," *Catalysis Today*, vol. 116, pp. 415–421, 2006.

[29]  S. J. Lee, J. McBreen, S. Mukerjee, E. A. Ticianelli, and R. C. Urian, "Electrocatalysis of CO Tolerance by Carbon-Supported PtMo Electrocatalysts in PEMFCs," *Journal of Electrochemical Society*, vol. 151, pp. A1094-A1103, 2004.

[30]  E. M. Assaf, M. S. Batista, E. I. Santiago, and E. A. Ticianelli, "Mechanism of CO Tolerance on Molybdenum-Based Electrocatalysts for PEMFC," *Journal of Electrochemical Society*, vol. 151 pp. A944-A949, 2004.

[31]  M. Iwase and S. Kawatsu, "Optimized CO tolerant electrocatalysts for polymer electrolyte fuel cells," *Proceedings of the First International Symposium on Proton Conducting Membrane Fuel Cells*, vol. 1, pp. 12–18, 1995.

[32]  F. A. de Bruijn, M. Keijzer, and D. C. Papageorgopoulos, "The inclusion of Mo, Nb and Ta in Pt and PtRu carbon supported electrocatalysts in the quest for improved CO tolerant PEMFC anodes," *Electrochimica Acta*, vol. 48, pp. 197–204, 2002.

[33]    V. A. Paganin, L. G. Pereira, M. E. Pereira, F. R. dos Santos, and E. A. Ticianelli, "CO tolerance effects of tungsten-based PEMFC anodes," *Electrochimica Acta*, vol. 51, pp. 4061–4066, 2006.

[34]    Data provided by Los Alamos National Lab, from fuel cell team headed by E. Brosha

[35]    K. P. Jong, *Synthesis of Solid Catalysts*, Weinheim: Wiley, 2009.

[36]    S. J. Pearton and R. J. Shul, *Handbook of Advanced Plasma Processing Techniques*, New York: Springer-Verlag, 2000.

[37]    B. Chapman, *Glow Discharge Processes: Sputtering and Plasma Etching.* New York: Wiley-Interscience, 1980.

[38]    A. J. Lichtenberg and M. A. Lieberman, *Principles of Plasma Discharges and Materials Processing*, 2nd ed. New York: Wiley Interscience, 2005.

[39]    F. Jansen and J. Mort, *Plasma Deposited Thin Films*. Boca Raton, Florida: CRC Press, 2000.

[40]    J. Phillips, "Plasma generation of supported metal catalysts," U.S. Patent 5 989 648, Nov. 23, 1999.

[41]    S. Carabineiro, I. M. Fonseca, J. Phillips, and S. Shim, "Plasma generation of supported metal catalysts," *Applied Catalysis A: General*, vol. 237, no. 1/2, pp. 41–51, Nov. 2002.

[42]    C. C. Luhrs, J. Phillips, and M. Richard, "Engineering Particles Using the Aerosol-Through-Plasma Method," *IEEE Transactions on Plasmas*, vol. 37, pp. 726–739, 2009.

[43]    C. K. Chen, S. Gleiman, and J. Phillips, "Low-power Plasma Torch Method for the Production of Crystalline Spherical Ceramic Particles," *Journal of Materials Research*, vol. 16, pp. 1256–1265, 2001.

[44]    C. H. Chou and J. Phillips, "Plasma Production of Metallic Nanoparticles," *Journal of Materials Research*, vol. 7, pp. 2107–2113, 1992.

[45]    C. K. Chen, A. Datye, I. Fonseca, K. Lester, A. Phillips, J. Phillips, and H. Zea, "Plasma torch generation of carbon supported metal catalysts," *Catalysis Today*, vol. 89, no. 1/2, pp. 237–244, Feb. 2004.

[46]    B. W. Jang and C. Shi, "Nonthermal RF plasma modifications on Pd/γ-Al2O3 for selective hydrogenation of acetylene in the presence of ethylene," *Industrial & Engineering Chemistry Research*, vol. 45, no. 17, pp. 5879–5884, 2006.

[47]    B. W. Jang, M. Macias, and C. Ratanatawanate, "Promotion effect of 842 the nonthermal RF plasma treatment on Ni/Al2O3 for benzene hydrogenation," *Industrial & Engineering Chemistry Research*, vol. 44, no. 26, pp. 9868–9874, 2005.

[49]    D. Cheng, B. W. Jang, C. Liu, Y. Han, C. Ratanatawanate, K. Yu, J. Zhan, and J. Zou, "Plasma application for more environmentally-friendly catalyst preparation," *Pure Applied Chemistry*, vol. 78, no. 6, pp. 1227–1238, 2006.

[49]    C. J. Liu, Y. P. Zhang, and J. J. Zou, "Control of the metal–support interface of NiO-loaded photocatalysts via cold plasma treatment," *Langmuir*, vol. 22, no. 5, pp. 2334–2339, 2006.

[50]    O. Kubaschewski and B. E. Hopkins, *Oxidation of Metals and Alloys*, London, U.K.: Butterworths, 1962.

[51]    B. D. Cullity, *Elements of X-Ray Diffraction*, Addison-Wesley Pub. Co. Inc, 1978.

[52]    S. Swapp, *Scanning Electron Microscopy (SEM)*, Wyoming: Integrating, 2012.

[53]    B. L. Gabriel, *SEM: A User's Manual for Materials Science*, Metals Park, Ohio: American Soceiety for Metals, 1985.

[54]    D. C. Joy, J. Goldstein, and A. D. Romig, *Principles of Analytical Electron Microscopy*, New York: Springer, 1986, 6th ed.

[55]    S. Brunauer, P. H. Emmett, and E. Teller, "Adsorption of Gases in Multimolecular Layers," *Journal of the American Chemistry Society*, vol. 60, pp. 309–319, 1938.

[56]    N. Hwang and A. Barron, "BET Surface Area Analysis," *Connexions*, vol. 2012, pp. May 8, 2011, 2001.

[57]    Quantachrome Instruments, *NOVAe Series High-Speed Surface Area and Pore Size Analyzers*, 2011.

THIS PAGE INTENTIONALLY LEFT BLANK

# INITIAL DISTRIBUTION LIST

1.      Defense Technical Information Center
        Ft. Belvoir, Virginia

2.      Dudley Knox Library
        Naval Postgraduate School
        Monterey, California